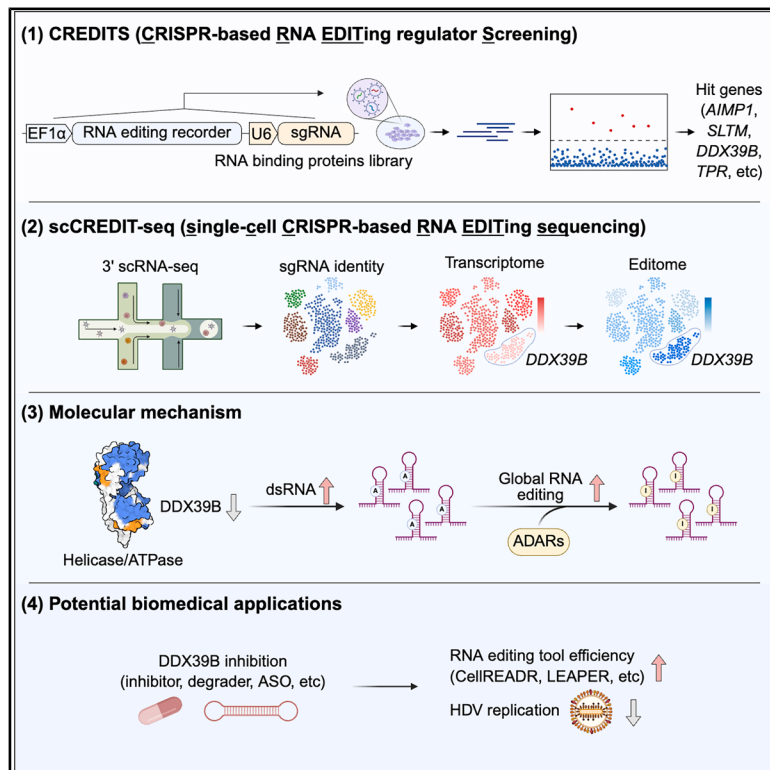


Multimodal CRISPR screens uncover DDX39B as a global repressor of A-to-I RNA editing

Graphical abstract



Authors

Tianzi Wei, Jiaxuan Li, Xiang Lei, ..., Zhenfeng Zhang, Shimin Shuai, Ruilin Tian

Correspondence

shuaism@sustech.edu.cn (S.S.), tianrl@sustech.edu.cn (R.T.)

In brief

Wei, Li, Lei et al. develop CREDITS and scCREDIT-seq, two complementary CRISPR-based platforms for systematic discovery of A-to-I RNA editing regulators. They identify DDX39B as a global repressor via dsRNA regulation and demonstrate its utility in enhancing RNA editing technologies and anti-HDV therapeutic strategies.

Highlights

- CREDITS, a pooled CRISPR screen platform for systematic discovery of RNA editing regulators
- scCREDIT-seq enables single-cell profiling of editome and transcriptome under perturbations
- DDX39B suppresses global A-to-I editing by resolving dsRNA
- Targeting DDX39B boosts RNA editing tool efficiency and disrupts HDV replication



Resource

Multimodal CRISPR screens uncover DDX39B as a global repressor of A-to-I RNA editing

Tianzi Wei,^{1,2,3,6} Jiaxuan Li,^{2,4,6} Xiang Lei,^{1,2,3,6} Risheng Lin,^{1,2,3} Qingyan Wu,⁵ Zhenfeng Zhang,⁵ Shimin Shuai,^{2,4,*} and Ruilin Tian^{1,2,3,7,*}

¹Department of Medical Neuroscience, School of Medicine, Southern University of Science and Technology, Shenzhen, Guangdong 518055, China

²SUSTech Homeostatic Medicine Institute, School of Medicine, Southern University of Science and Technology, Shenzhen, Guangdong 518055, China

³Key University Laboratory of Metabolism and Health of Guangdong, Southern University of Science and Technology, Shenzhen, Guangdong 518055, China

⁴Department of Human Cell Biology and Genetics, School of Medicine, Southern University of Science and Technology, Shenzhen, Guangdong 518055, China

⁵School of Public Health and Emergency Management, Southern University of Science and Technology, Shenzhen, Guangdong 518055, China

⁶These authors contributed equally

⁷Lead contact

*Correspondence: shuaism@sustech.edu.cn (S.S.), tianrl@sustech.edu.cn (R.T.)

<https://doi.org/10.1016/j.celrep.2025.116009>

SUMMARY

Adenosine-to-inosine (A-to-I) RNA editing is a critical post-transcriptional modification that diversifies the transcriptome and influences various cellular processes, yet its regulatory mechanisms remain largely unknown. Here, we present two complementary CRISPR-based genetic screening platforms: CREDITS (CRISPR-based RNA editing regulator screening), which enables genome-scale identification of editing regulators using an RNA recorder-based reporter system, and scCREDIT-seq (single-cell CRISPR-based RNA editing sequencing), which provides multiplexed single-cell characterization of transcriptome and editome changes for pooled perturbations. By screening 1,350 RNA-binding proteins, we identified a series of A-to-I editing regulators. Mechanistic investigation revealed DDX39B as a global repressor of A-to-I editing, which functions by preventing double-stranded RNA accumulation through its helicase activity. Targeting DDX39B significantly enhances the efficiency of RNA-editing-based tools, such as CellREADR (cell access through RNA sensing by endogenous ADAR) and LEAPER (leveraging endogenous ADAR for programmable editing of RNA), and disrupts hepatitis D virus (HDV) RNA editing homeostasis. These technological advances not only expand our understanding of RNA editing regulation but also provide powerful tools for exploring tissue-specific and context-dependent RNA modification mechanisms, with broad implications for therapeutic development.

INTRODUCTION

Adenosine-to-inosine (A-to-I) editing is a prevalent post-transcriptional RNA modification in which ADAR (adenosine deaminase acting on RNA) enzymes convert adenosine to inosine through hydrolytic deamination. Inosine is recognized as guanosine by cellular machinery, effectively recoding genetic information and enhancing transcriptome diversity.^{1–4}

The ADAR family comprises three main proteins in mammals: ADAR1 (ADAR), which exists in two isoforms (p150 and p110) ubiquitously expressed in all tissues; ADAR2 (ADARB1), which is primarily expressed in the brain; and ADAR3 (ADARB2), which is catalytically inactive but may have regulatory roles. These enzymes target double-stranded RNA (dsRNA) regions formed by inverted repeat sequences, complementary se-

quences in adjacent introns, or complex RNA secondary structures.^{5–7}

Recent advances in high-throughput sequencing technologies have led to the identification of millions of A-to-I editing sites (the editome) across the human transcriptome, revealing its widespread occurrence in both coding and non-coding regions.^{8–12} In coding sequences, editing can lead to amino acid recoding, potentially altering protein function. In non-coding regions, editing can affect RNA splicing, stability, and localization.

The precise spatiotemporal regulation of A-to-I editing is crucial for maintaining cellular function and homeostasis, as exemplified in neural function and immune response regulation. In the nervous system, editing modifies neurotransmitter receptors, regulates synaptic transmission, and influences neural development.^{13–16} Within the immune system, A-to-I editing



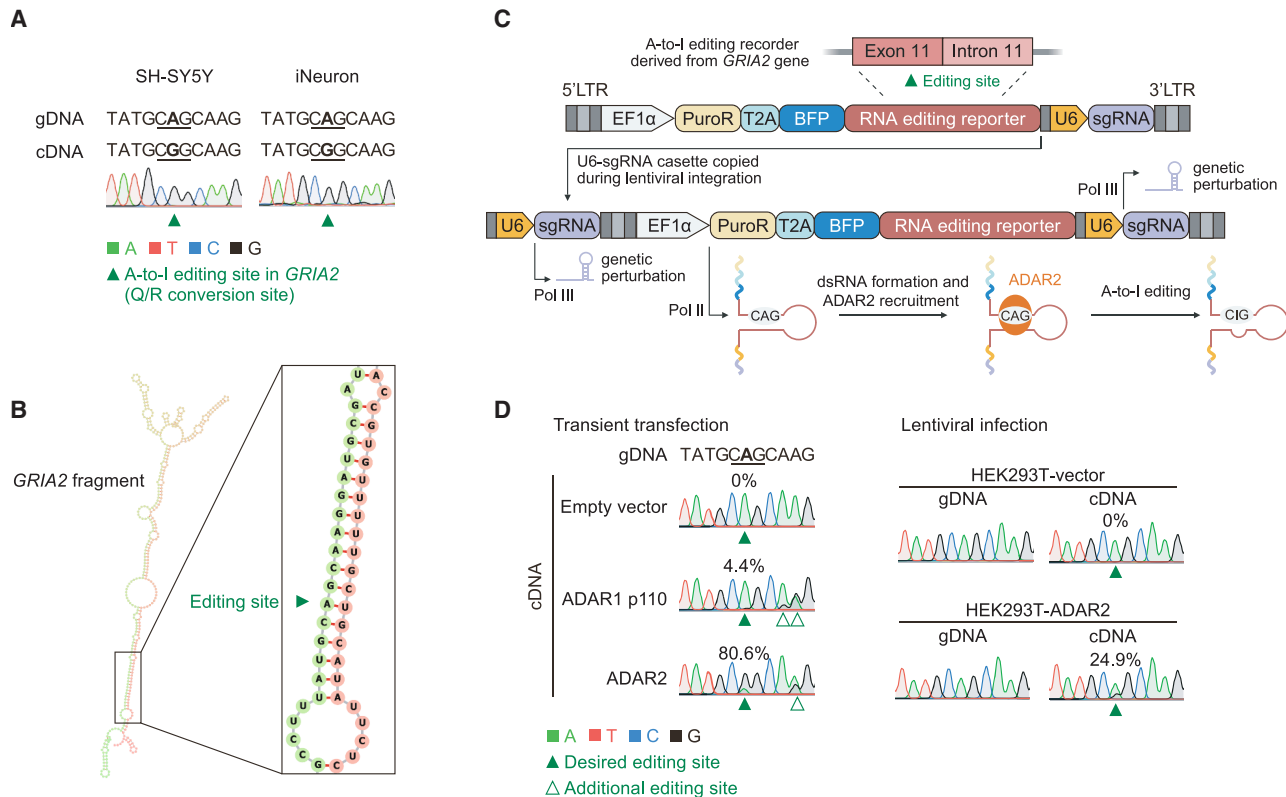


Figure 1. Development of CREDITS vector

(A) Sanger sequencing electropherograms showing A-to-G conversion at the *GRIA2* Q/R site in SH-SY5Y cells and human iPSC-derived neurons (iNeurons). (B) Predicted RNA secondary structure of the *GRIA2* fragment (chr4:157336674–157337074, hg38) using the RNAfold web server. (C) Schematic of the CREDITS vector design. The *GRIA2*-derived A-to-I editing recorder is inserted into a CROP-seq vector (pMK1334), with the EF1 α promoter driving the co-transcription of the recorder and sgRNA sequence. (D) Sanger sequencing electropherograms showing A-to-G conversions in the CREDITS recorder in cells expressing ADAR1/2 via transient transfection (left) or lentiviral infection (right).

plays crucial roles in viral RNA modification, innate immunity regulation, and the discrimination between self and non-self RNA.^{17–20} Dysregulation of RNA editing has been associated with numerous diseases, such as cancer, neurological disorders, and autoimmune diseases.^{21–25}

Recent efforts have identified additional A-to-I regulators beyond the well-characterized ADAR proteins.^{8,26–31} Yet, the complex regulatory network controlling editing efficiency and specificity remains poorly understood. Discovering new A-to-I regulators holds promise for advancing our understanding of RNA editing mechanisms, improving RNA-editing-based technologies for programmable RNA modifications and targeted cell manipulation, and developing therapeutics for related diseases.

Here, we established high-throughput CRISPR-based genetic screening platforms that enable systematic identification and multiplexed transcriptome and editome characterization of A-to-I RNA editing regulators. Through these technologies, we uncovered multiple previously unknown regulators of A-to-I editing and elucidated the role of DDX39B as a global repressor of A-to-I editing. We further demonstrated targeting DDX39B as a potential strategy to enhance RNA-editing-based tools and develop antiviral therapies.

RESULTS

Development of CREDITS for pooled CRISPR screening on A-to-I editing

To enable pooled CRISPR screening for A-to-I editing regulators, we developed a method called CREDITS (CRISPR-based RNA editing regulator screening). The general principle of this method is to associate sgRNA-induced genetic perturbations with the A-to-I editing outcomes of an RNA editing recorder. We reasoned that an RNA fragment that contains known editing sites in a dsRNA structure could serve as a molecular recorder for A-to-I editing events. One of the well-established A-to-I editing sites in human cells is the Q/R conversion site in the *GRIA2* gene.¹⁴ We validated the endogenous editing of this site in a neuroblastoma cell line, SH-SY5Y, and in induced pluripotent stem cell (iPSC)-derived neurons (Figure 1A), consistent with previous reports that the Q/R conversion event of *GRIA2* is catalyzed by ADAR2, which is expressed mostly in neuronal cells.^{15,32} Therefore, a fragment of *GRIA2* containing the Q/R conversion site and the flanking sequences predicted to form a dsRNA structure was used as a candidate RNA editing recorder for further characterization (Figure 1B). The editing outcomes of the recorder can be

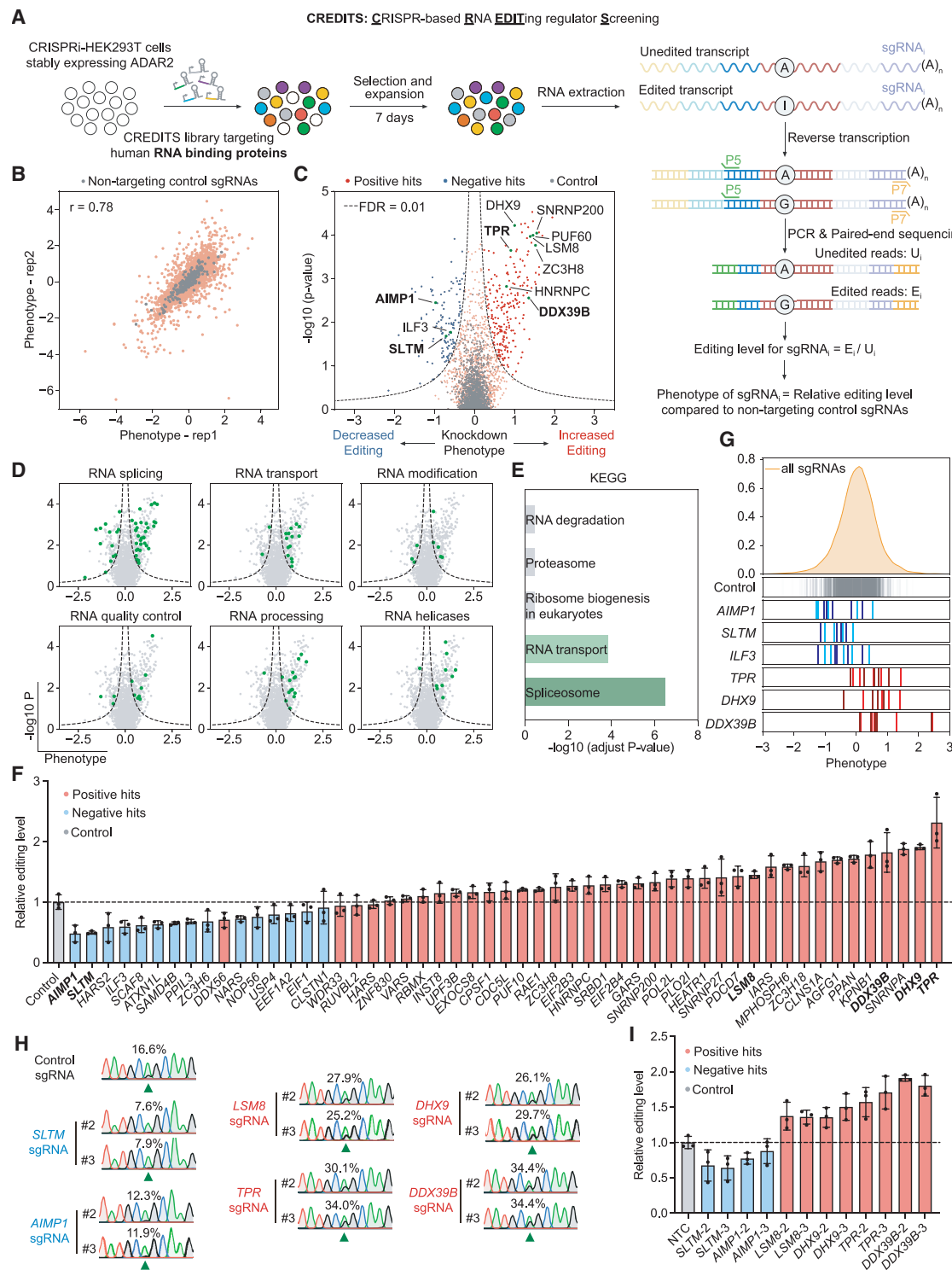


Figure 2. An RBP-focused CREDITS screen identifies known and novel RNA editing regulators

(A) Screening strategy of CREDITS. HEK293T cells stably expressing ADAR2 and the CRISPRi machinery were transduced with an sgRNA library targeting 1,350 human RNA-binding proteins (MOI < 0.3). Following puromycin selection and cell expansion, total RNA was extracted and reverse transcribed. A 1,018-bp region containing both the editing recorder and sgRNA sequence was PCR amplified to generate an NGS library for paired-end sequencing. For each sgRNA_i, the editing level was calculated as the ratio of edited reads (E) to unedited reads (U). The phenotype score for each sgRNA_i was determined by normalizing its editing level to the median editing level of non-targeting control sgRNAs. The screen was performed in two independent biological replicates.

(legend continued on next page)

retrieved by Sanger sequencing or next-generation sequencing (NGS), as A-to-I editing events lead to A-to-G conversions in RT-PCR.

We inserted this A-to-I editing recorder into a previously published CROP-seq vector (pMK1334),³³ resulting in the CREDITS vector in which the recorder can be co-transcribed with sequences containing sgRNA identity from an EF1a promoter, in addition to the U6 promoter-driven sgRNA expression for gene perturbation. Thereby, the effect of a specific genetic perturbation on A-to-I editing can be associated with the editing outcomes of the recorder (Figure 1C). Importantly, the recorder region in the full-length CREDITS transcript is predicted to preserve the dsRNA structure (Figure S1A).

To test the performance of the CREDITS vector, we transiently transfected HEK293T cells with the CREDITS vector containing a non-targeting control sgRNA. Additionally, the cells were cotransfected with either an ADAR1 p110 or ADAR2 overexpression vector or an empty vector. Following RNA extraction and reverse transcription, the recorder region was PCR amplified and subjected to Sanger sequencing. A strong A-to-I editing signal at the desired site in the recorder was detected in cells overexpressing ADAR2, whereas no or minimal editing can be detected in cells overexpressing either an empty vector or ADAR1 p110 (Figure 1D). This is as expected because the Q/R conversion site in *GRI/A2* is specific to ADAR2,^{15,32} which is minimally expressed in HEK293T cells.^{34,35} Interestingly, we observed additional editing signals at adjacent adenosines in cells overexpressing ADAR1 p110 and ADAR2, potentially due to high levels of transiently expressed ADAR proteins. To avoid “off-target” editing, we sought to lower the level of ADAR2 overexpression by lentiviral delivery of an ADAR2 expression cassette into the HEK293T cells, generating the HEK293T-ADAR2 cell line (Figures S1B–S1D). The CREDITS vector was also delivered by lentivirus into the HEK293T-ADAR2 cells (Figure S1E). As expected, a clear A-to-I editing signal was detected specifically at the desired site, with no off-target editing sites detected (Figure 1D). Moreover, no editing was detected in the genomic DNA of the recorder region, ruling out the possibility that the recorder was pre-edited during lentiviral production and infection prior to genome integration. Taking these results together, we established a sequencing-based reporter system that is suitable for pooled high-throughput CRISPR screening on A-to-I editing regulation.

A CREDITS screen uncovered novel A-to-I RNA editing regulators

We next developed a HEK293T cell line that stably expresses ADAR2 along with the CRISPRi machinery (dCas9-BFP-KRAB),

designated as CRISPRi-HEK293T-ADAR2. Using this cell line, we conducted a focused CRISPRi screen to identify factors that regulate A-to-I RNA editing. We constructed a CREDITS library containing 6,602 sgRNAs targeting 1,350 RNA-binding proteins (RBPs) and 250 non-targeting control sgRNAs. The CREDITS library was introduced into the CRISPRi-HEK293T-ADAR2 cells through lentiviral infection. Following selection and expansion, we extracted total RNA from the cells and performed reverse transcription. We then PCR amplified the region containing both the RNA editing recorder and the sgRNA sequence to generate an NGS library for paired-end sequencing (Figure 2A). From each read pair, Read2 was used to identify the sgRNA identity, while Read1 was used to reveal the editing outcome of the recorder. The recorder editing level for each sgRNA was calculated as the ratio of edited to unedited read counts, and the phenotype of each sgRNA was determined as its relative editing level compared to non-targeting control sgRNAs (Figure 2A; STAR Methods). The strong correlation ($r = 0.78$) between phenotype scores from duplicate screens indicated the robustness and reproducibility of our screen (Figure 2B).

The screen identified 225 positive hits and 119 negative hits (false discovery rate [FDR] < 0.01) whose knockdown increased or decreased the A-to-I editing of the recorder, respectively (Figure 2C; Table S1). These hits are involved in diverse RNA-related processes, including splicing, transport, modification, quality control, RNA processing, and RNA helicase activity (Figure 2D). Notably, our screen uncovered previously reported genes involved in A-to-I regulation, such as *ILF3*,²⁸ *PUF60*,³¹ *HNRNPC*,³¹ *SNRNP200*,³¹ *ZC3H8*,³¹ and *DHX9*,²⁶ validating the robustness of our screen. KEGG enrichment analysis revealed that positive hits were significantly enriched in spliceosome and RNA transport pathways (Figure 2E), in line with previous reports that inhibiting RNA splicing led to increased A-to-I editing.^{36,37}

Intriguingly, the screen uncovered many hit genes that have not been previously associated with A-to-I editing. To validate these findings, we selected 53 hits (38 positive and 15 negative) for individual validation, encompassing both known and potentially novel A-to-I regulators. We individually cloned sgRNAs targeting these genes into the CREDITS vector and introduced them into CRISPRi-HEK293T-ADAR2 cells. Sanger sequencing analysis of the recorder’s editing outcomes showed remarkable consistency with the initial screen: all negative hits (15/15) and most positive hits (34/38) reproduced their respective effects on A-to-I editing (Figures 2F and 2G). The phenotypes of 6 selected genes that showed a strong effect in both the initial screen and first-round validation—*SLTM*, *AIMP1*, *LSM8*, *TPR*,

(B) Scatterplot showing correlation of phenotype scores between two biological replicates ($r = 0.78$).

(C) Volcano plots showing knockdown phenotypes and statistical significance (Mann-Whitney U test) for genes targeted in the pooled screen. Screening results were analyzed by the MAGeCK-iNC pipeline. Dashed lines: cutoff for hit genes (FDR = 0.01). Known and novel hits discussed in the paper are labeled, and novel hits are highlighted in bold.

(D) Classification of hit genes based on RNA-related pathways.

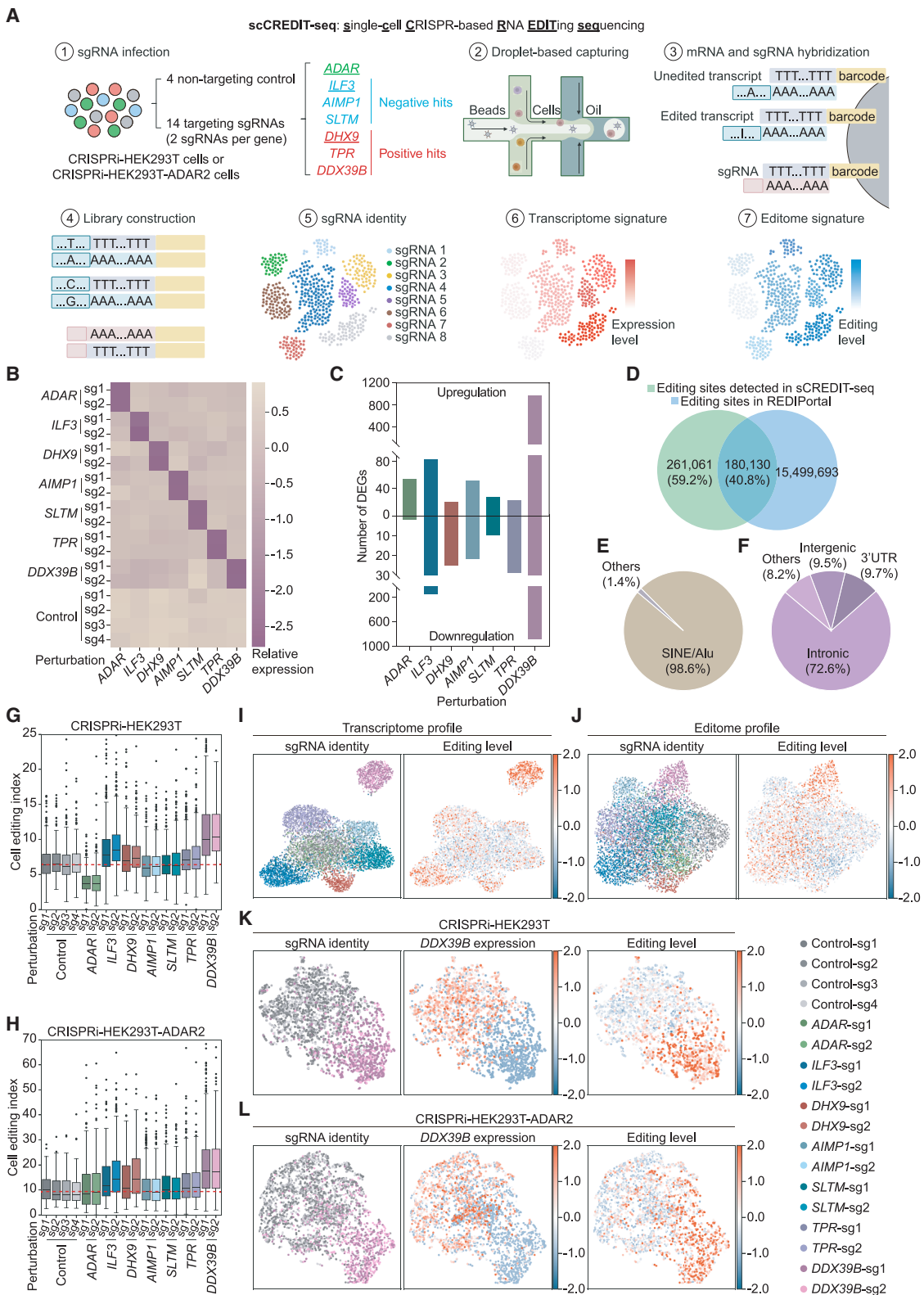
(E) KEGG enrichment analysis for positive hits. Significant enriched signaling pathways are marked in green.

(F) Individual validation of hit genes from the primary screen using Sanger sequencing (mean \pm SD, $n = 3$ technical replicates). One sgRNA was cloned for each hit. Editing levels were normalized to that of the control sgRNA. Hit genes selected for secondary validation are highlighted in bold.

(G) Distributions of phenotype scores for non-targeting control sgRNAs and sgRNAs targeting selected negative (blue) and positive (red) hits.

(H and I) Validation of editing phenotypes for selected hits using Sanger sequencing with two additional sgRNAs per gene. (H) Representative electropherograms.

(I) Quantification of editing levels relative to control sgRNAs (mean \pm SD, $n = 3$ technical replicates).



(legend on next page)

DXH9, and *DDX39B*—were further confirmed using two additional sgRNAs (Figures 2H and 2I). Quantitative PCR (qPCR) and immunoblotting analyses showed that the knockdown of the top hit genes—*SLTM*, *AIMP1*, *DDX39B*, and *TPR*—did not affect ADAR2 mRNA and protein levels, suggesting that their effects are not mediated through regulating ADAR2 expression (Figures S1F and S1G).

In summary, our screen uncovered known and potentially novel A-to-I RNA editing regulators, highlighting CREDITS as a robust platform for systematic investigation of RNA editing regulation.

Development of scCREDIT-seq for scalable RNA editome-wide characterization of gene perturbations

Coupling CRISPR screening with single-cell omics enables screens on complex high-dimensional phenotypes. Technologies like CROP-seq and Perturb-seq, for instance, integrate CRISPR screening with single-cell RNA sequencing (scRNA-seq), allowing for transcriptome-wide characterization of gene perturbations at the single-cell level.^{38–41}

Our initial screen relied on an exogenous reporter system. To examine whether and how the hit genes modulate A-to-I editing of endogenous RNAs, we developed scCREDIT-seq (single-cell CRISPR-based RNA editing sequencing). This method leverages scRNA-seq to simultaneously profile sgRNA identity, gene expression signatures, and A-to-I editing signatures at single-cell resolution. This approach enables high-throughput multiplexed characterization of transcriptome and editome changes across pooled CRISPR perturbations.

The scCREDIT-seq workflow is similar to CROP-seq and is compatible with most 3' scRNA-seq chemistries but uniquely incorporates a computational pipeline for quantifying RNA editing levels at single-cell resolution (Figure 3A; STAR Methods). Briefly, sgRNAs are cloned into the CROP-seq vector pMK1334, which generates polyadenylated sgRNA-containing transcripts, allowing for sgRNA detection via scRNA-seq. A pooled collection of cells expressing different sgRNAs is processed using a droplet-based capturing method, enabling the simultaneous capture of mRNA and polyadenylated sgRNA-containing transcripts from individual cells. During library construction, A-to-I editing events in the captured transcripts result in A-to-G conversions in the final library. The sgRNA-containing transcripts are additionally amplified and sequenced as previously described to facilitate sgRNA identity assignment.^{33,40,42,43} Following sequencing, bioinformatic an-

alyses are conducted to link sgRNA identity with gene expression and A-to-I editing profiles and to determine transcriptome and editome changes associated with each perturbation.

For our proof-of-principle scCREDIT-seq screen, we selected seven genes representing both known and novel regulators of A-to-I editing. As a positive control, we included *ADAR*, which encodes ADAR1, one of the primary enzymes responsible for catalyzing A-to-I editing. We selected another six genes from our initial screen: three positive hits (*DHX9*, *TPR*, and *DDX39B*) and three negative hits (*ILF3*, *AIMP1*, and *SLTM*). Among these, *ILF3*²⁸ and *DHX9*²⁶ had previously reported roles in A-to-I editing, while the other four genes (*TPR*, *DDX39B*, *AIMP1*, and *SLTM*) represent novel regulators identified through our screen. A total of 18 sgRNAs (two sgRNAs targeting each selected gene and four non-targeting control sgRNAs) were cloned into pMK1334, forming the scCREDIT-seq screen library. Parallel screens were conducted in HEK293T cells expressing the CRISPRi machinery with or without ADAR2 overexpression (CRISPRi-HEK293T-ADAR2 and CRISPRi-HEK293T, respectively). Approximately 20,000 cells were processed for each scCREDIT-seq screen, and totals of 7,147 and 5,838 cells were retained after quality control for screens in CRISPRi-HEK293T and CRISPRi-HEK293T-ADAR2 cells, respectively. Since both screens yielded similar conclusions, we focused on the results from the CRISPRi-HEK293T cells, as they represent a more native context, unless otherwise specified.

While most scRNA-seq methods use oligo-dT primers to target polyadenylated transcripts, these approaches can capture sequences beyond the 3' end due to secondary priming positions throughout transcripts. Previous studies have shown that up to 25% of scRNA-seq reads may contain intronic or other gene body sequences.⁴⁴ Analysis of our scCREDIT-seq data confirmed this observation: while reads were enriched at the 3' end, we detected substantial coverage across gene bodies and intergenic regions (Figure S2A), suggesting that our approach can capture editing events throughout transcripts, despite the inherent bias of the sequencing method.

We confirmed the effective knockdown of all target genes in cells expressing the respective sgRNAs (Figures 3B and S2B). To determine gene expression changes induced by each perturbation, we performed pseudobulk differential gene expression analysis using DESeq2 with aggregated counts for each sgRNA. We found that *DDX39B* knockdown induced the most dramatic

Figure 3. Single-cell transcriptome and editome characterization of A-to-I RNA editing regulators using scCREDIT-seq

- (A) Schematic of the scCREDIT-seq workflow.
- (B) Heatmap showing on-target knockdown efficiency for each sgRNA in the scCREDIT-seq screen.
- (C) Number of up- and downregulated differentially expressed genes (DEGs) in each perturbation.
- (D) Venn diagram showing the overlap between A-to-I editing sites identified by scCREDIT-seq analysis and known editing sites documented in the REDIportal database.
- (E and F) Genomic distribution of high-confidence RNA editing sites identified from the scCREDIT-seq, categorized by repetitive element type (E) and genomic region (F).
- (G and H) Boxplots showing cell editing index (CEI) in cells expressing different sgRNAs in CRISPRi-HEK293T (G) and CRISPRi-HEK293T-ADAR2 (H) cells. The red dashed line represents the median CEI of the control cells.
- (I and J) UMAP visualization of the scCREDIT-seq data following linear discriminant analysis (LDA) on transcriptome profile (I) or editome profile (J), color coded by sgRNAs. The color legend representing each sgRNA is shown (bottom).
- (K and L) UMAP visualization of a subset of the scCREDIT-seq data that contain only *DDX39B* sgRNAs and control sgRNAs following LDA in CRISPRi-HEK293T (K) and CRISPRi-HEK293T-ADAR2 (L) cells.

transcriptome changes, with 980 upregulated and 882 downregulated genes (Figure 3C).

We developed a computational pipeline to identify A-to-I RNA editing sites from scRNA-seq data (STAR Methods). Briefly, sequencing reads were aligned to the reference human genome, and A-to-G mismatches were identified from the BAM files as potential A-to-I editing sites. These sites were then stringently filtered based on reads, cell representations, and common genomic SNPs. Comparison with the REDIportal database⁴⁵ revealed that of the 441,191 editing sites detected by scCREDIT-seq, 180,130 (40.8%) matched previously reported sites, while 261,061 (59.2%) were novel (Figure 3D). We considered the overlapping sites as high-confidence A-to-I editing sites and focused our subsequent analysis on these sites.

Analysis of the genomic distribution of identified editing sites revealed that the vast majority (98.6%) of them were located within *Alu* repeats, a class of SINE (short interspersed element) retroelements (Figure 3E). These sites were predominantly found in intronic regions (72.6%), followed by 3' untranslated regions (3' UTRs; 9.7%) (Figure 3F). A similar genomic distribution of identified editing sites from scCREDIT-seq in CRISPRi-HEK293T-ADAR2 cells was observed as well (Figures S2C and S2D). This distribution pattern aligns with previous studies showing that *Alu* repeats, which are abundant in introns and 3' UTRs, serve as hotspots for A-to-I editing,^{46–48} thus validating our approach. While most perturbations did not significantly affect the genomic distribution of editing sites, ADAR knockdown resulted in a slight increase in the proportion of editing events within 3' UTRs (Figures S2E and S2F).

To evaluate how gene perturbations affect global RNA editing, we developed a cell editing index (CEI) to quantify overall editing levels in single cells (STAR Methods). Analysis of CEI distributions showed that sgRNAs targeting the same gene produced similar effects, demonstrating high data reproducibility (Figures 3G and 3H). As expected, ADAR knockdown markedly decreased CEI levels, while ADAR2 overexpression in CRISPRi-HEK293T-ADAR2 cells reversed this effect. Knockdown of all three positive hits—*DHX9*, *TPR*, and *DDX39B*—increased CEI levels, indicating their influence extends beyond the reporter to overall editing. Notably, *DDX39B* knockdown caused a dramatic increase in CEI levels in both CRISPRi-HEK293T and CRISPRi-HEK293T-ADAR2 cells, suggesting its strong regulatory role in global A-to-I editing.

Among the negative hits (*ILF3*, *AIMP1*, and *SLTM*), none showed decreased overall editing upon knockdown. Interestingly, the knockdown of *ILF3* led to notable increases in global editing levels, contrasting with its effect on the reporter in our initial screen but consistent with its reported role as a negative regulator of RNA editing.²⁸ This finding suggests that *ILF3* may exert site-specific effects on A-to-I editing, highlighting the value of scCREDIT-seq as a complementary approach to CREDITS for comprehensive editome characterization.

To map the landscapes of gene expression and A-to-I editing across different perturbations, we performed linear discriminant analysis (LDA), a supervised dimensionality reduction method that can maximize discrimination between different perturbations, followed by uniform manifold approximation and projection (UMAP) visualization. This analysis revealed distinct

molecular signatures in both the transcriptome and editome for each perturbation (Figures 3I, 3J, S2G, and S2H). Notably, *DDX39B* knockdown cells formed distinct clusters in both analyses, consistent with our findings that *DDX39B* knockdown induced the most pronounced overall transcriptome and editome changes among all perturbations. The same patterns persisted when the *DDX39B* perturbation was analyzed separately against control sgRNAs (Figures 3K and 3L).

Analysis of a publicly available genome-wide Perturb-seq dataset (BioProject: PRJNA831566)⁴⁹ further validates our findings: cells with *DDX39B* knockdown displayed higher mean CEI values compared to control cells (Figure S2I), despite the fact that only a limited number of *DDX39B*-targeting cells remained after filtering.

To determine the minimal cell coverage required for scCREDIT-seq, we performed a bootstrap analysis. We found that for perturbation with strong effects, such as *ADAR* or *DDX39B*, as few as 50 cells are sufficient to robustly distinguish them from control sgRNAs. In contrast, for perturbations with moderate effects, such as *ILF3*, more than 100 cells are needed (Figure S3).

In conclusion, we established scCREDIT-seq as a scalable and robust method for multiplexed characterization of transcriptome and editome changes for pooled CRISPR perturbations and identified *DDX39B* as a novel global repressor of A-to-I editing.

Bulk RNA-seq confirms *DDX39B* as a global repressor of A-to-I RNA editing

To validate our scCREDIT-seq findings and further characterize how *DDX39B* knockdown affects A-to-I editing at different sites, we performed bulk RNA-seq on total RNAs from CRISPRi-HEK293T cells and CRISPRi-HEK293T-ADAR2 cells expressing either a control sgRNA or a *DDX39B*-targeting sgRNA. A-to-I editing sites were identified using the REDITools pipeline,⁵⁰ and only those that were also included in REDIportal were retained for downstream analysis.

As expected, A-to-I editing sites were predominantly found within *Alu* repeat regions (Figure 4A), with the majority located in intronic regions (53.5%) and 3' UTRs (20.0%) (Figure 4B). Among all mismatches identified, the frequency of A-to-G was significantly higher than those of other mismatches, such as A-to-T and A-to-C, which were negligible, confirming the detection of *bona fide* A-to-I events rather than technical artifacts. Knockdown of *DDX39B* significantly elevated overall A-to-I editing levels as measured by increased A-to-G conversions,⁵¹ while A-to-T and A-to-C conversions remained unchanged (Figure 4C), indicating a specific regulatory role of *DDX39B* on A-to-I editing rather than a global effect on RNA or DNA fidelity.

Next, we assessed A-to-I editing changes at the site level. As expected, ADAR2 overexpression significantly increased the number of up-edited sites, yielding an up-edited-to-down-edited site ratio of 2.21 (Figure 4D). Remarkably, *DDX39B* knockdown massively enhanced editing at over 80% of detected A-to-I sites, resulting in up-to-down ratios of 4.51 in CRISPRi-HEK293T cells and 7.12 in CRISPRi-HEK293T-ADAR2 cells (Figures 4E and 4F). In contrast, the ratios between two biological replicates were close to 1 (Figures S4A and S4B). These findings were further

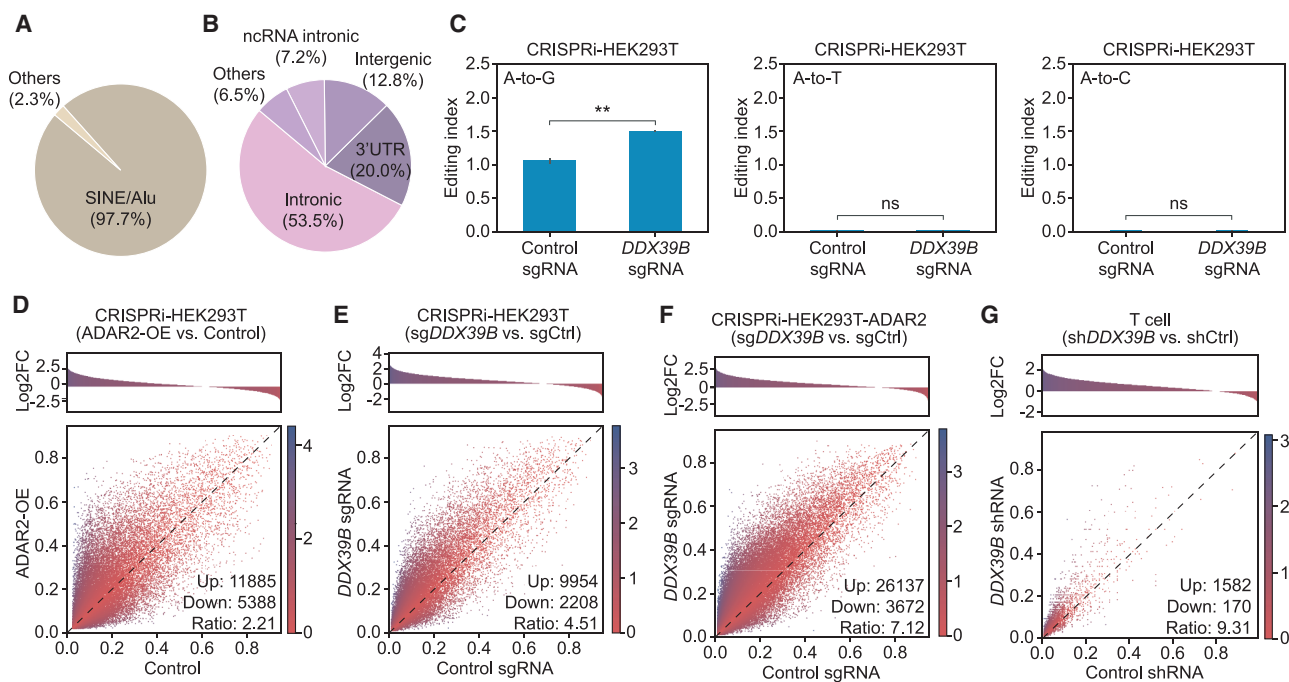


Figure 4. Bulk RNA-seq validation of DDX39B as a global repressor of RNA editing

(A and B) Genomic distribution of A-to-I RNA editing sites detected from bulk RNA-seq, categorized by repetitive element type (A) and genomic region (B). (C) Histograms showing the A-to-G (left), A-to-T (middle), and A-to-C (right) conversion indices calculated by RNAEditingIndexer.⁵¹ The A-to-G editing index is significantly higher in DDX39B knockdown cells compared to that of control cells. *p* value is calculated by Student's *t* test. ***p* < 0.01; ns, not significant. (D) Differential RNA editing analysis between control and ADAR2-overexpressing (ADAR2-OE) cells at consensus editing sites. (Top) Histogram showing the distribution of log2 fold changes (log2FCs) in editing levels (ADAR2-OE/control). (Bottom) Scatterplot comparing editing levels between control (x axis) and ADAR2-OE (y axis) cells, where each dot represents an individual editing site. Color bar representing log2FC is shown. Numbers of up-edited and down-edited sites (|log2FC| > 0.5) and their ratios are indicated. (E–G) Differential RNA editing analysis for DDX39B knockdown in CRISPRi-HEK293T cells (E), CRISPRi-HEK293T-ADAR2 cells (F), and T cells (G). RNA-seq data for T cells was obtained from GEO: GSE145773.⁵²

supported by independent analysis using a recently reported computational method, LoDEI⁵³ (Figure S4C).

Consistent with previous reports,^{54–56} we observed a very weak correlation between differential gene expression and RNA editing levels (Figure S4D; Spearman's rho = -0.031, *p* = 0.020). Furthermore, a comparison of DDX39B knockdown effects on transcriptome and editome measured by bulk RNA-seq and scCREDIT-seq demonstrated high concordance across datasets (Figures S4E and S4F), supporting the robustness of our single-cell screening approach.

To validate the effect of DDX39B in other cell types, we analyzed published RNA-seq datasets for DDX39B knockdown in T cells (GEO: GSE145773⁵²) and HeLa cells (GEO: GSE94730⁵⁷). Consistently, DDX39B knockdown in these cells also significantly promoted global A-to-I editing (Figures 4G and S4G).

To determine whether this regulation is shared by other RNA helicases, we examined DHX9—another DEAD-box family member identified in our screen (Figures 2C and 2F)—using DHX9 knockdown RNA-seq data from GEO: GSE99789.²⁶ Unlike DDX39B, DHX9 depletion had a bidirectional effect, with roughly equal numbers of editing sites increasing or decreasing (Figure S4H), consistent with DHX9's previously described dual role in RNA editing.²⁶

Together, these results demonstrate that DDX39B functions as a relatively specific global repressor of A-to-I editing, supporting the findings from our scCREDIT-seq screen.

DDX39B interacts with ADAR1 in an RNA-dependent manner without altering ADAR1 expression or localization

To investigate how DDX39B regulates A-to-I editing, we first examined whether it affects the levels of ADAR proteins. RNA-seq and qPCR analyses demonstrated that the knockdown of DDX39B did not affect the mRNA expression levels of ADAR, ADARB1, or ADARB2 (Figures S5A and S5B). Western blot analyses showed that neither DDX39B knockdown nor its overexpression affected ADAR1 levels in HEK293T cells (Figures 5A and 5B). Next, we investigated whether DDX39B physically interacts with ADAR1. Co-immunoprecipitation experiments revealed a strong association between DDX39B and ADAR1, which was diminished upon RNase A treatment (Figure 5C), indicating that DDX39B interacts with ADAR1 in an RNA-dependent manner.

Next, we examined the subcellular localization of DDX39B and ADARs. We generated a HEK293T cell line with its endogenous DDX39B locus tagged with a green fluorescence protein, mNeonGreen, at the N terminus via CRISPR-Cas9-mediated

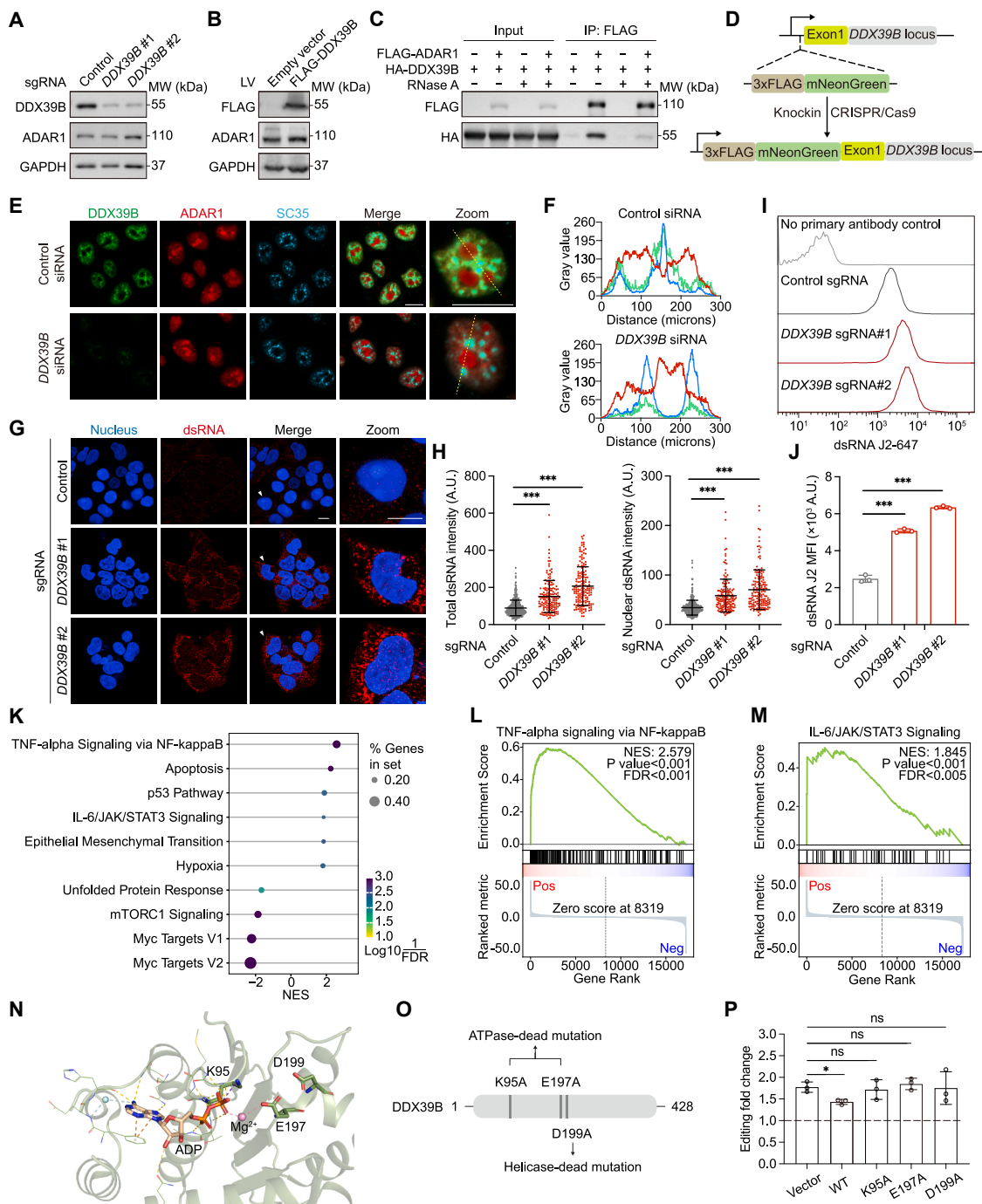


Figure 5. DDX39B regulates RNA editing through its helicase and ATPase activities

- (A) Western blot showing protein levels of DDX39B and ADAR1 in control and *DDX39B* knockdown CRISPRi-HEK293T cells. GAPDH was used as the loading control.
- (B) Western blot showing the levels of FLAG-DDX39B and ADAR1 proteins in CRISPRi-HEK293T cells with the overexpression of empty vector or FLAG-DDX39B. GAPDH was used as the loading control.
- (C) Co-immunoprecipitation analysis showing the physical interaction between FLAG-ADAR1 (p110 isoform) and HA-DDX39B with or without RNase A treatment.
- (D) Schematic of the generation of mNeonGreen-DDX39B HEK293T cells by CRISPR/Cas9-mediated knockin.
- (E) Immunofluorescence showing the localization of DDX39B (green), ADAR1 (red), and SC35 (cyan) in mNeonGreen-DDX39B HEK293T cells transfected with control or *DDX39B*-targeting siRNAs.

(legend continued on next page)

homologous recombination (Figure 5D). Immunofluorescence (IF) analyses in these cells showed that both DDX39B and ADAR1 were localized in the nucleus (Figures 5E and S5C). Consistent with previous reports,⁵⁸ ADAR1 was distributed throughout the nucleus, with a strong enrichment in the nucleolus. DDX39B, however, was localized in the nucleoplasm and enriched in nuclear speckles (stained by SC35) but was excluded from the nucleolus, suggesting that DDX39B may interact with ADAR1 in the nucleoplasm or nuclear speckle, where they were co-localized. ADAR2 showed similar localization patterns to ADAR1 when overexpressed in HEK293T cells (Figures S5C and S5D). The localization and subnuclear distribution of ADAR1 remained unchanged upon *DDX39B* knockdown in HEK293T cells (Figures 5E and 5F). Together, these findings excluded the possibility that DDX39B regulates A-to-I editing by modulating ADAR expression or localization.

DDX39B regulates A-to-I editing through its helicase and ATPase activities

DDX39B is a member of the DEAD-box RNA helicase family, catalyzing dsRNA unwinding and promoting R-loop clearance.^{59–63} We hypothesized that the knockdown of *DDX39B* may lead to dsRNA accumulation, thus providing more substrates for A-to-I editing. To test this, we measured the dsRNA levels in control and *DDX39B* knockdown cells using the J2 antibody, which specifically recognizes dsRNAs. Indeed, *DDX39B* knockdown dramatically increased dsRNA levels in the cell, as measured by IF and flow cytometry (Figures 5G–J). The accumulation of dsRNAs in the cell will stimulate the innate immune response.^{64,65} In agreement with this, upregulated DEGs from the RNA-seq analyses of *DDX39B* knockdown showed strong enrichment in the immunity- and inflammation-related pathways, including tumor necrosis factor alpha (TNF- α) signaling via nuclear factor κ B (NF- κ B) and interleukin (IL)-6/JAK/STAT3 signaling (Figures 5K–M). Cell-death-related pathways, including apoptosis and the p53 pathway, were also enriched (Figure 5K), consistent with previous reports that dsRNA accumulation can trigger cell death.^{66,67} Using a cell viability assay, we confirmed that prolonged *DDX39B* suppression induced cytotoxic effects (Figure S5E).

The RNA helicase activity of DDX39B is dependent on its ATPase activity.^{61,63,68} Previous mutagenesis studies have identified that K95 and E197 residues are essential for its ATPase ac-

tivity and D199 is essential for its helicase function^{52,61,63} (Figures 5N and 5O). To dissect whether these enzymatic activities are required for the function of DDX39B in regulating A-to-I editing, we transduced wild-type (WT), ATPase-dead (K95A and E197A), and helicase-dead (D199A) mutants of DDX39B into CRISPRi-HEK293T-ADAR2 cells expressing a CREDITS vector with either a control sgRNA or an sgRNA targeting *DDX39B* (Figure S6A). We found that only WT DDX39B could partially revert the effect of increased A-to-I editing caused by *DDX39B* knockdown, whereas ATPase-dead or helicase-dead mutants failed to rescue this phenotype (Figures 5P, S6B, and S6C).

The indispensable role of the enzymatic activity of DDX39B in A-to-I regulation was further validated at the editome level through bulk RNA-seq analysis of *DDX39B* knockdown cells transduced with an empty BFP vector, WT DDX39B, or the enzymatic-dead E197A DDX39B mutant. Editome analysis confirmed that only WT DDX39B, not the E197A mutant, could reverse the upregulated overall editing levels induced by *DDX39B* knockdown (Figures S6D–S6F).

In summary, our findings suggest that DDX39B regulates A-to-I editing potentially by preventing dsRNA formation through its helicase and ATPase activities.

Targeting DDX39B improves RNA-editing-based tool efficiency

Having established DDX39B as a potent repressor of A-to-I editing, we explored its potential as a target to enhance the efficiency of existing RNA-editing-based tools. CellREADR (cell access through RNA sensing by endogenous ADAR) is a cell monitoring and manipulation tool that couples RNA detection with the expression of effector proteins, relying on A-to-I editing.⁶⁹ To monitor the efficiency of CellREADR, we implemented a dual-fluorescence reporter system similar to that described in the original publication (Figure 6A). The reporter consists of a UbC-promoter-driven transcript containing mCherry, a sense-edit-switch RNA (sesRNA), and EGFP. While mCherry is constitutively expressed, EGFP expression requires sesRNA hybridization to its target RNA. This hybridization recruits ADAR proteins, which edit an in-frame UAG stop codon in the sesRNA to a UIG tryptophan codon, enabling downstream translation. Thus, the efficiency of CellREADR can be quantified by measuring the EGFP/mCherry ratio. We generated CellREADR vectors for five previously validated sesRNAs targeting human

(F) Quantitative analysis of co-localization of DDX39B (green), ADAR1 (red), and SC35 (cyan) in mNeonGreen-DDX39B HEK293T cells transfected with control (top) or *DDX39B*-targeting siRNAs (bottom).

(G) Representative immunofluorescence images of dsRNA staining by the J2 antibody (red) in control and *DDX39B* knockdown HEK293T cells. Nuclei were counterstained with DAPI. Scale bar: 20 μ m.

(H) Quantitative analysis of fluorescent intensity of dsRNA staining in whole cells (left) and in the nucleus (right). *** p < 0.001 by unpaired two-sided Student's t test.

(I) and (J) Flow cytometry analysis of intracellular dsRNA levels in control and *DDX39B* knockdown CRISPRi-HEK293T cells. Representative flow cytometry histograms (I) showing dsRNA detection using J2 antibody staining. (J) Quantification of mean fluorescence intensity (MFI) from J2 staining (mean \pm SD, n = 3 biological replicates). *** p < 0.001 by unpaired two-sided Student's t test.

(K–M) Gene set enrichment analysis (GSEA) of DEGs in *DDX39B* knockdown cells (K). TNF- α signaling via NF- κ B (FDR < 0.001, L) and IL-6/JAK/STAT3 signaling (FDR < 0.005, M) pathways were significantly upregulated.

(N) 3D structure of DDX39B highlighting the ATP-Mg²⁺-binding pocket (PDB: 1XTJ).

(O) Schematic of ATPase-dead and helicase-dead mutations in DDX39B.

(P) Rescue experiments showing RNA editing levels of the CREDITS reporter in *DDX39B* knockdown cells transfected with wild-type (WT) or enzymatic mutant DDX39B. Data were normalized to control cells and presented as fold change (mean \pm SD, n = 3 biological replicates). p values from unpaired two-sided Student's t test. * p < 0.05; ns, not significant.

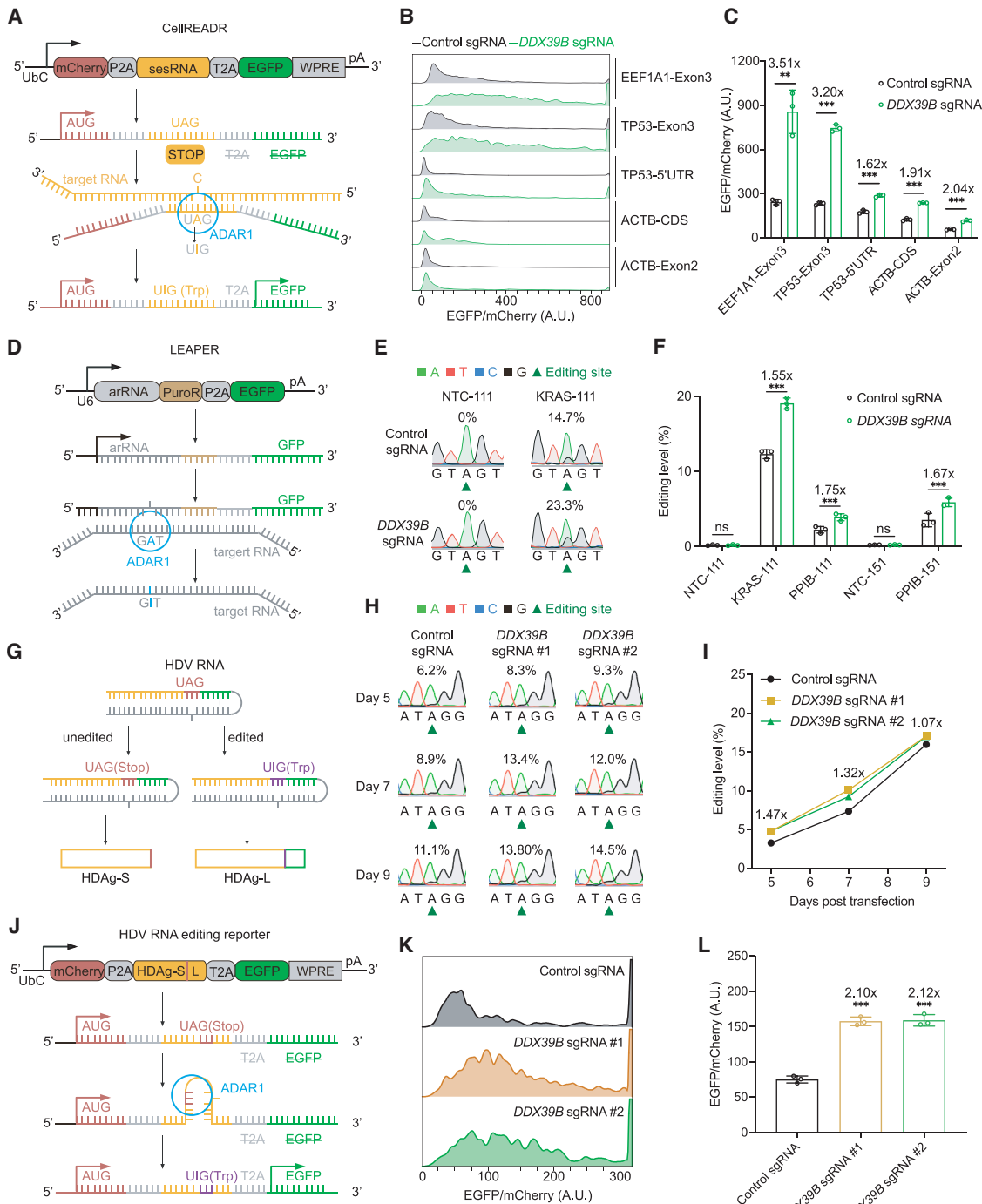


Figure 6. Targeting *DDX39B* as a strategy for improving RNA-editing-based tools and developing anti-HDV therapy

(A) Schematic showing the dual-fluorescence reporter for CellREADR.

(B) Flow cytometry analysis of CellREADR editing efficiency (EGFP/mCherry intensity ratios) in control and *DDX39B* knockdown cells.

(C) Quantification of CellREADR efficiency by flow cytometry (mean ± SD, n = 3 biological replicates). **p < 0.01 and ***p < 0.001 by unpaired two-sided Student's t test. Fold changes are indicated.

(D) Schematic illustration of LEAPER arRNA targeting an endogenous transcript.

(E) Sanger sequencing electropherograms showing A-to-G conversion at the LEAPER target site in control and *DDX39B* knockdown cells.

(F) NGS quantification of editing rates at targeted adenosines in KRAS and PP1B transcripts using arRNAs of varying lengths (mean ± SD, n = 3 biological replicates). p values from unpaired two-sided Student's t test. ***p < 0.001; ns, not significant. Fold changes are indicated.

(G) Schematic illustration of A-to-I editing in HDV RNA. ADAR1-mediated editing at the amber/W site extends HDAg-S to produce HDAg-L.

(legend continued on next page)

EEF1A1 exon 3, *TP53* exon 3, *TP53* 5' UTR, *ACTB* CDS, and *ACTB* exon 2. These vectors were transfected into CRISPRi-HEK293T cells expressing either a control or *DDX39B*-targeting sgRNA. Intriguingly, the knockdown of *DDX39B* substantially increased EGFP/mCherry ratios by up to 3.51-fold across all CellREADR constructs as measured by flow cytometry (Figures 6B, 6C, and S7A). These findings indicate that targeting *DDX39B* could enhance CellREADR efficiency.

LEAPER (leveraging endogenous ADAR for programmable editing of RNA) is another tool that employs a short, engineered ADAR-recruiting RNA (arRNA) to recruit endogenous ADAR proteins for targeted A-to-I editing.^{70,71} We generated vectors expressing previously validated arRNAs targeting endogenous *KRAS* and *PPIB* transcripts (Figure 6D) and transfected them into control and *DDX39B* knockdown CRISPRi-HEK293T cells. The transfected cells were sorted by fluorescence-activated cell sorting (FACS), and the editing levels of the target RNAs were determined by Sanger sequencing and NGS. Notably, knocking down *DDX39B* significantly improved target RNA editing across all arRNAs tested (Figures 6E and 6F), suggesting that targeting *DDX39B* could also enhance LEAPER efficiency.

Taken together, these results demonstrate the potential of targeting *DDX39B* as a strategy for improving RNA-editing-based tools.

Targeting *DDX39B* disrupts HDV RNA editing homeostasis and replication

While A-to-I editing plays a crucial role in regulating host antiviral immunity, certain viruses have evolved to exploit the host's A-to-I editing machinery to facilitate their life cycle. A notable example is the hepatitis D virus (HDV), which possesses a single-stranded circular RNA genome of approximately 1,700 nucleotides that folds into a unique rod-like structure through extensive base pairing. The genome encodes only one protein, the HDV antigen (HDAg), which exists in two isoforms: HDAg-S (small) and HDAg-L (large), which are essential for viral replication and viral particle assembly, respectively. The switch from HDAg-S to HDAg-L relies on host ADAR1-mediated A-to-I RNA editing at a specific site known as the amber/W site,^{72,73} resulting in a 19- to 20-amino-acid extension at the C terminus (Figure 6G). Maintaining a balanced level of A-to-I editing is critical for viral persistence, as HDAg-L, while necessary for viral particle secretion, strongly inhibits HDV replication. Therefore, modulating A-to-I editing represents a promising strategy for anti-HDV therapeutic development.

To investigate whether targeting *DDX39B* could influence A-to-I editing in the HDV genome, we transiently transfected a vector expressing the HDV RNA genome into control and *DDX39B* knockdown CRISPRi-HEK293T cells. At various time

points post-transfection, we assessed the A-to-I editing levels at the amber/W site in the HDV genome using Sanger sequencing and NGS. In control cells, we detected A-to-I editing at the amber/W site in a time-dependent manner (Figures 6H and 6I) that resembled the phenomenon seen during live virus infection,⁷⁴ thus validating our approach. Intriguingly, knockdown of *DDX39B* markedly increased A-to-I editing levels in HDV RNA across all time points (Figures 6H and 6I). This effect was further validated using a dual-fluorescence reporter system analogous to the one used for CellREADR but with the sesRNA sequence replaced with the HDAg sequence (Figure 6J). In this reporter, EGFP expression requires A-to-I editing of an in-frame UAG stop codon in HDAg to UIG. Flow cytometry analysis revealed that *DDX39B* knockdown significantly increased the EGFP/mCherry ratio in CRISPRi-HEK293T cells expressing the reporter (Figures 6K and 6L).

To evaluate the anti-HDV effect of *DDX39B* inhibition, we performed a viral infection experiment: HepG2 cells overexpressing HDV receptor NTCP (designated as HepG2-NTCP cells) were transfected with control or *DDX39B*-targeting small interfering RNAs (siRNAs) and subsequently infected with HDV. RT-qPCR and IF analyses demonstrated that *DDX39B* suppression markedly reduced HDV RNA levels and HDAg expression in HDV-infected HepG2-NTCP cells (Figures S7B–S7E).

Collectively, these findings demonstrate that *DDX39B* suppression enhances A-to-I editing in the HDV RNA and impairs HDV replication.

DISCUSSION

In this study, we developed two complementary CRISPR-based screening platforms to systematically identify and characterize key regulators of A-to-I RNA editing: CREDITS, which enables genome-scale screens using a reporter system, and scCREDIT-seq, which provides single-cell editome characterization for focused gene sets. Applying these platforms to screen 1,350 human RBPs, we uncovered multiple known and novel A-to-I regulators. Through detailed mechanistic investigation of one novel regulator, the RNA helicase *DDX39B*, we elucidated that it represses global A-to-I editing by preventing dsRNA accumulation. We also demonstrated that targeting *DDX39B* enhances RNA-editing-based tools and impairs HDV replication.

While the enzymatic mechanism of A-to-I editing by ADAR proteins is well characterized, the cellular mechanisms governing the precise spatiotemporal control of editing events remain largely unknown. Previous efforts to identify RNA editing regulators have primarily employed three strategies: correlation analyses between genetic variants or gene expression and RNA editing levels,^{8,75} editome analyses of publicly available or

(H) Sanger sequencing electropherograms showing A-to-G conversion in HDV RNA from control and *DDX39B* knockdown cells. Target adenosine is highlighted.
(I) Time-course analysis of HDV RNA editing levels in control and *DDX39B* knockdown cells by NGS. Average fold changes are indicated.

(J) Schematic of a dual-fluorescence reporter for measuring HDV genome A-to-I editing. The reporter replaces sesRNA in CellREADR with the HDV genome, triggering EGFP expression upon editing.

(K and L) Flow cytometry analysis of HDV reporter editing efficiency (EGFP/mCherry intensity ratios) in control and *DDX39B* knockdown HEK293T cells. (K) Representative flow cytometry histograms showing the distribution of EGFP/mCherry intensity ratio. (L) Quantification of HDV reporter editing efficiency in control and *DDX39B* knockdown CRISPRi-HEK293T cells (mean \pm SD, $n = 3$ biological replicates). *** $p < 0.001$ by unpaired two-sided Student's t test. Fold changes are indicated.

in-house bulk RNA-seq data from various gene perturbations,^{31,76} and proteomics and biochemical analyses of ADAR-interacting proteins.^{26–28} Our platforms introduce a genetic screening approach to studying A-to-I editing, offering a systematic method to explore this regulatory landscape.

Our CREDITS method offers several key advantages. First, it enables NGS-based RNA-level readout by directly linking an RNA recorder to sgRNA, which is more straightforward and effective compared to fluorescence-based strategies that require converting RNA-level phenotypes into fluorescent signals and subsequent cell sorting for screening. This capability is particularly beneficial for cell types that are difficult to sort, such as neurons. Second, the method is highly versatile: although the CREDITS screen in this study used an ADAR2-dependent A-to-I editing recorder, CREDITS can be readily adapted to study diverse DNA or RNA phenotypes—including ADAR1-mediated RNA editing, RNA splicing, and other RNA modifications—simply by changing the recorder sequence. Indeed, similar screening approaches have successfully identified modulators of prime editing^{77,78} and RNA m⁵C modification.⁷⁹

The integration of single-cell technologies has transformed CRISPR screening by enabling complex high-dimensional phenotypes as readouts. Technologies such as Perturb-seq and CROP-seq focus on transcriptome responses, while the recently developed PerturbSci-Kinetics⁴¹ analyzes transcriptome kinetics, and CPA-Perturb-seq⁸⁰ examines poly(A) site usage. Our scCREDIT-seq method further expands the toolbox by providing a scalable method that can simultaneously assess transcriptome and editome changes for pooled genetic perturbations. Complementing the single-reporter-based CREDITS approach, scCREDIT-seq enables unbiased, transcriptome-wide characterization to determine whether the effects of gene perturbations on RNA editing are site specific or global.

DDX39B is a multifaceted RNA helicase involved in processes such as RNA splicing and RNA export.^{59,60} It plays important roles in development and disease pathogenesis, including T cell fate determination,⁵² neurodevelopmental diseases,⁸¹ and tumorigenesis.^{82–84} Our study suggests that DDX39B prevents dsRNA accumulation and thereby represses A-to-I editing. Future investigations are needed to determine the precise mechanisms by which DDX39B regulates RNA editing and how this function contributes to its roles in both normal physiology and disease contexts.

RNA-editing-based tools like CellREADR and LEAPER provide powerful approaches for manipulating cellular function and correcting disease-causing mutations. Our work demonstrates that targeting DDX39B can enhance the efficiency of these tools. However, as DDX39B inhibition leads to widespread A-to-I editing changes, achieving site specificity remains a key challenge. A promising approach involves fusing a dominant-negative variant of DDX39B with ADAR to enable local enhancement of RNA editing at the intended target sites.

Additionally, we demonstrated that targeting DDX39B increases RNA editing of the HDV genome and inhibits viral replication. However, prolonged DDX39B inhibition reduces cell viability; therefore, developing strategies for transient or localized DDX39B inhibition will be critical to exploiting this pathway for therapeutic intervention while minimizing cytotoxicity.

We anticipate that our screening platforms can be broadly applied to various cell types and conditions to decipher tissue-specific and context-dependent regulation of A-to-I editing, thereby advancing our understanding of RNA modification mechanisms, promoting the development of RNA-modification-related technologies, and facilitating the development of therapeutic strategies for associated diseases.

Limitations of the study

This study has several limitations. First, we screened only 1,350 RBPs using the RBP library, which may have overlooked other important A-to-I regulators; future studies employing alternative or genome-wide libraries will be necessary to identify additional factors. Second, although we showed that DDX39B's helicase activity is critical for its repression of A-to-I editing, the detailed molecular mechanism by which it interfaces with ADAR proteins and dsRNA remains unknown. Third, while targeting DDX39B enhanced the performance of RNA editing tools and blocked HDV replication, more refined approaches will be needed to achieve site-specific editing without widespread off-target effects. Finally, our CREDITS and scCREDIT-seq screens were conducted solely in HEK293T cells; expanding these platforms to other cell types and physiological contexts will be essential for understanding tissue- and context-dependent regulation of A-to-I editing.

RESOURCE AVAILABILITY

Lead contact

Further information and requests for resources and reagents should be directed to and will be fulfilled by the lead contact, Ruilin Tian (tianrl@sustech.edu.cn).

Materials availability

This study did not generate new unique reagents.

Data and code availability

- The raw sequence data reported in this paper have been deposited in the Genome Sequence Archive⁸⁵ in National Genomics Data Center⁸⁶ China National Center for Bioinformation/Beijing Institute of Genomics, Chinese Academy of Sciences (GSA-Human: HRA011402), and are accessible at <https://ngdc.cncb.ac.cn/gsa-human/browse/HRA011402>.
- All original code is available on Zenodo (<https://doi.org/10.5281/zendoo.15614476>) and publicly available as of the date of publication.
- Any additional information required to reanalyze the data reported in this paper is available from the [lead contact](#) upon request.

ACKNOWLEDGMENTS

We acknowledge Dr. Hao Chen (School of Medicine, SUSTech) for his insightful discussions and valuable suggestions, which contributed to this study. This work was supported by the National Key Research and Development Program of China (2024YFA0919800), the Shenzhen Medical Research Fund (A2303039 to R.T. and A2303044 to S.S.), the Guangdong Basic and Applied Basic Research Foundation (2023B1515020075 to R.T.), the Shenzhen Fundamental Research Program (JCYJ20220530112602006 and RCYX20221008092845052 to R.T.), the National Natural Science Foundation of China (32100766 and 82171416 to R.T., 82270239 to S.S., and 32400478 to T.W.), and the China Postdoctoral Science Foundation (2023M731523 to T.W.). We thank Dr. Xibin Lu for his guidance of FACS in SUSTech Core Research Facilities. We also acknowledge the Center for Computational Science and Engineering at SUSTech for computational resources.

AUTHOR CONTRIBUTIONS

T.W., J.L., X.L., S.S., and R.T. contributed to the study's overall conception, design, and interpretation and wrote the manuscript and created the figures with input from the other authors. T.W. designed and conducted the screens of CREDITS and scCREDIT-seq and validated the screening results and investigated the molecular mechanisms under the supervision of R.T. J.L. analyzed the scCREDIT-seq and bulk RNA-seq data with guidance from S.S. and R.T. R.L. established the mNeonGreen-tagged *DDX39B* cell line. X.L. designed and conducted the experiments related to RNA-editing-based tools. Q.W. and Z.Z. performed the experiments related to HDV infection. All authors reviewed and had the opportunity to comment on the paper.

DECLARATION OF INTERESTS

The authors declare no competing interests.

STAR★METHODS

Detailed methods are provided in the online version of this paper and include the following:

- KEY RESOURCES TABLE
- EXPERIMENTAL MODEL AND STUDY PARTICIPANT DETAILS
 - Cell culture
 - HDV
- METHOD DETAILS
 - Plasmid and siRNA transfection
 - Generation of CREDITS vector
 - Generation of CRISPRi-HEK293T cell line with the stable overexpression of ADAR2
 - Detection of RNA editing in CREDITS vector by sanger sequencing
 - CRISPRi screening with CREDITS and data analysis
 - Primary validation of screening hits
 - Quantitative real-time PCR (qRT-PCR)
 - Immunoblotting
 - Co-immunoprecipitation (Co-IP)
 - scCREDIT-seq and data analysis
 - RNA sequencing (RNA-seq) and data analysis
 - Correlation analysis
 - mNeonGreen knock-in for *DDX39B* in HEK293T
 - Immunofluorescence (IF)
 - Detection of dsRNA accumulation
 - Protein structure analysis and site mutagenesis
 - Generation of CellREADR vector and data analysis
 - Generation of LEAPER vector and data analysis
 - HDV assays
- QUANTIFICATION AND STATISTICAL ANALYSIS

SUPPLEMENTAL INFORMATION

Supplemental information can be found online at <https://doi.org/10.1016/j.celrep.2025.116009>.

Received: December 31, 2024

Revised: May 9, 2025

Accepted: June 24, 2025

REFERENCES

1. Walkley, C.R., and Li, J.B. (2017). Rewriting the transcriptome: adenosine-to-inosine RNA editing by ADARs. *Genome Biol.* 18, 205. <https://doi.org/10.1186/s13059-017-1347-3>.
2. Cui, L., Ma, R., Cai, J., Guo, C., Chen, Z., Yao, L., Wang, Y., Fan, R., Wang, X., and Shi, Y. (2022). RNA modifications: importance in immune cell biology and related diseases. *Signal Transduct. Target. Ther.* 7, 334. <https://doi.org/10.1038/s41392-022-01175-9>.
3. Slotkin, W., and Nishikura, K. (2013). Adenosine-to-inosine RNA editing and human disease. *Genome Med.* 5, 105. <https://doi.org/10.1186/gm508>.
4. Zipeto, M.A., Jiang, Q., Melese, E., and Jamieson, C.H.M. (2015). RNA rewriting, recoding, and rewiring in human disease. *Trends Mol. Med.* 21, 549–559. <https://doi.org/10.1016/j.molmed.2015.07.001>.
5. Rehwinkel, J., and Mehdipour, P. (2025). ADAR1: from basic mechanisms to inhibitors. *Trends Cell Biol.* 35, 59–73. <https://doi.org/10.1016/j.tcb.2024.06.006>.
6. Savva, Y.A., Rieder, L.E., and Reenan, R.A. (2012). The ADAR protein family. *Genome Biol.* 13, 252. <https://doi.org/10.1186/gb-2012-13-12-252>.
7. Matthews, M.M., Thomas, J.M., Zheng, Y., Tran, K., Phelps, K.J., Scott, A.I., Havel, J., Fisher, A.J., and Beal, P.A. (2016). Structures of human ADAR2 bound to dsRNA reveal base-flipping mechanism and basis for site selectivity. *Nat. Struct. Mol. Biol.* 23, 426–433. <https://doi.org/10.1038/nsmb.3203>.
8. Tan, M.H., Li, Q., Shanmugam, R., Piskol, R., Kohler, J., Young, A.N., Liu, K.I., Zhang, R., Ramaswami, G., Ariyoshi, K., et al. (2017). Dynamic landscape and regulation of RNA editing in mammals. *Nature* 550, 249–254. <https://doi.org/10.1038/nature24041>.
9. Wang, F., He, J., Liu, S., Gao, A., Yang, L., Sun, G., Ding, W., Li, C.Y., Gou, F., He, M., et al. (2021). A comprehensive RNA editome reveals that edited Azin1 partners with DDX1 to enable hematopoietic stem cell differentiation. *Blood* 138, 1939–1952. <https://doi.org/10.1182/blood.2021011314>.
10. Eisenberg, E., and Levanon, E.Y. (2018). A-to-I RNA editing - immune protector and transcriptome diversifier. *Nat. Rev. Genet.* 19, 473–490. <https://doi.org/10.1038/s41576-018-0006-1>.
11. Nishikura, K. (2016). A-to-I editing of coding and non-coding RNAs by ADARs. *Nat. Rev. Mol. Cell Biol.* 17, 83–96. <https://doi.org/10.1038/nrm.2015.4>.
12. Liu, Z., Quinones-Valdez, G., Fu, T., Huang, E., Choudhury, M., Reese, F., Mortazavi, A., and Xiao, X. (2023). L-GIREMI uncovers RNA editing sites in long-read RNA-seq. *Genome Biol.* 24, 171. <https://doi.org/10.1186/s13059-023-03012-w>.
13. Behm, M., and Öhman, M. (2016). RNA Editing: A Contributor to Neuronal Dynamics in the Mammalian Brain. *Trends Genet.* 32, 165–175. <https://doi.org/10.1016/j.tig.2015.12.005>.
14. Sommer, B., Köhler, M., Sprengel, R., and Seuberg, P.H. (1991). RNA editing in brain controls a determinant of ion flow in glutamate-gated channels. *Cell* 67, 11–19. [https://doi.org/10.1016/0092-8674\(91\)90568-j](https://doi.org/10.1016/0092-8674(91)90568-j).
15. Higuchi, M., Maas, S., Single, F.N., Hartner, J., Rozov, A., Burnashev, N., Feldmeyer, D., Sprengel, R., and Seuberg, P.H. (2000). Point mutation in an AMPA receptor gene rescues lethality in mice deficient in the RNA-editing enzyme ADAR2. *Nature* 406, 78–81. <https://doi.org/10.1038/35017558>.
16. Burns, C.M., Chu, H., Rueter, S.M., Hutchinson, L.K., Canton, H., Sanders-Bush, E., and Emeson, R.B. (1997). Regulation of serotonin-2C receptor G-protein coupling by RNA editing. *Nature* 387, 303–308. <https://doi.org/10.1038/387303a0>.
17. Di Giorgio, S., Martignano, F., Torcia, M.G., Mattiuz, G., and Conticello, S.G. (2020). Evidence for host-dependent RNA editing in the transcriptome of SARS-CoV-2. *Sci. Adv.* 6, eabb5813. <https://doi.org/10.1126/sciadv.abb5813>.
18. Polson, A.G., Bass, B.L., and Casey, J.L. (1996). RNA editing of hepatitis delta virus antigenome by dsRNA-adenosine deaminase. *Nature* 380, 454–456. <https://doi.org/10.1038/380454a0>.
19. Liddicoat, B.J., Piskol, R., Chalk, A.M., Ramaswami, G., Higuchi, M., Hartner, J.C., Li, J.B., Seuberg, P.H., and Walkley, C.R. (2015). RNA

- editing by ADAR1 prevents MDA5 sensing of endogenous dsRNA as nonself. *Science* 349, 1115–1120. <https://doi.org/10.1126/science.aac7049>.
20. Quin, J., Sedmik, J., Vukić, D., Khan, A., Keegan, L.P., and O'Connell, M. A. (2021). ADAR RNA Modifications, the Epitranscriptome and Innate Immunity. *Trends Biochem. Sci.* 46, 758–771. <https://doi.org/10.1016/j.tibs.2021.02.002>.
 21. Hwang, T., Park, C.K., Leung, A.K.L., Gao, Y., Hyde, T.M., Kleinman, J.E., Rajpurohit, A., Tao, R., Shin, J.H., and Weinberger, D.R. (2016). Dynamic regulation of RNA editing in human brain development and disease. *Nat. Neurosci.* 19, 1093–1099. <https://doi.org/10.1038/nn.4337>.
 22. Cheng, H., Yu, J., and Wong, C.C. (2025). Adenosine-to-Inosine RNA editing in cancer: molecular mechanisms and downstream targets. *Protein Cell* 16, 391–417. <https://doi.org/10.1093/procel/pwae039>.
 23. Chen, L., Li, Y., Lin, C.H., Chan, T.H.M., Chow, R.K.K., Song, Y., Liu, M., Yuan, Y.F., Fu, L., Kong, K.L., et al. (2013). Recoding RNA editing of AZIN1 predisposes to hepatocellular carcinoma. *Nat. Med.* 19, 209–216. <https://doi.org/10.1038/nm.3043>.
 24. Roth, S.H., Danan-Gothold, M., Ben-Izhak, M., Rechavi, G., Cohen, C. J., Louzoun, Y., and Levanon, E.Y. (2018). Increased RNA Editing May Provide a Source for Autoantigens in Systemic Lupus Erythematosus. *Cell Rep.* 23, 50–57. <https://doi.org/10.1016/j.celrep.2018.03.036>.
 25. Li, Q., Gloudemann, M.J., Geisinger, J.M., Fan, B., Aguet, F., Sun, T., Ramaswami, G., Li, Y.I., Ma, J.B., Pritchard, J.K., et al. (2022). RNA editing underlies genetic risk of common inflammatory diseases. *Nature* 608, 569–577. <https://doi.org/10.1038/s41586-022-05052-x>.
 26. Hong, H., An, O., Chan, T.H.M., Ng, V.H.E., Kwok, H.S., Lin, J.S., Qi, L., Han, J., Tay, D.J.T., Tang, S.J., et al. (2018). Bidirectional regulation of adenosine-to-inosine (A-to-I) RNA editing by DEAH box helicase 9 (DHX9) in cancer. *Nucleic Acids Res.* 46, 7953–7969. <https://doi.org/10.1093/nar/gky396>.
 27. Han, J., An, O., Hong, H., Chan, T.H.M., Song, Y., Shen, H., Tang, S.J., Lin, J.S., Ng, V.H.E., Tay, D.J.T., et al. (2020). Suppression of adenosine-to-inosine (A-to-I) RNA editome by death associated protein 3 (DAP3) promotes cancer progression. *Sci. Adv.* 6, eaaba5136. <https://doi.org/10.1126/sciadv.eaba5136>.
 28. Freund, E.C., Sapiro, A.L., Li, Q., Linder, S., Moresco, J.J., Yates, J.R., 3rd, and Li, J.B. (2020). Unbiased Identification of trans Regulators of ADAR and A-to-I RNA Editing. *Cell Rep.* 31, 107656. <https://doi.org/10.1016/j.celrep.2020.107656>.
 29. Koganti, P., Kadali, V.N., Manikoth Ayyathan, D., Emanuelli, A., Paolini, B., Levy-Cohen, G., and Blank, M. (2022). The E3 ubiquitin ligase SMURF2 stabilizes RNA editase ADAR1p110 and promotes its adenosine-to-inosine (A-to-I) editing function. *Cell. Mol. Life Sci.* 79, 237. <https://doi.org/10.1007/s00018-022-04272-8>.
 30. Shih, C.Y., Chen, Y.C., Lin, H.Y., and Chu, C.Y. (2023). RNA Helicase DDX6 Regulates A-to-I Editing and Neuronal Differentiation in Human Cells. *Int. J. Mol. Sci.* 24, 3197. <https://doi.org/10.3390/ijms24043197>.
 31. Quinones-Valdez, G., Tran, S.S., Jun, H.I., Bahn, J.H., Yang, E.W., Zhan, L., Brümmer, A., Wei, X., Van Nostrand, E.L., Pratt, G.A., et al. (2019). Regulation of RNA editing by RNA-binding proteins in human cells. *Commun. Biol.* 2, 19. <https://doi.org/10.1038/s42003-018-0271-8>.
 32. Melcher, T., Maas, S., Herb, A., Sprengel, R., Seeburg, P.H., and Higuchi, M. (1996). A mammalian RNA editing enzyme. *Nature* 379, 460–464. <https://doi.org/10.1038/379460a0>.
 33. Tian, R., Gachechiladze, M.A., Ludwig, C.H., Laurie, M.T., Hong, J.Y., Nathaniel, D., Prabhu, A.V., Fernandopulle, M.S., Patel, R., Abshari, M., et al. (2019). CRISPR Interference-Based Platform for Multimodal Genetic Screens in Human iPSC-Derived Neurons. *Neuron* 104, 239–255.e12. <https://doi.org/10.1016/j.neuron.2019.07.014>.
 34. Zambrano-Mila, M.S., Witzenberger, M., Rosenwasser, Z., Uzonyi, A., Nir, R., Ben-Aroya, S., Levanon, E.Y., and Schwartz, S. (2023). Dissecting the basis for differential substrate specificity of ADAR1 and ADAR2. *Nat. Commun.* 14, 8212. <https://doi.org/10.1038/s41467-023-43633-0>.
 35. Schaffer, A.A., Kopel, E., Hendel, A., Picardi, E., Levanon, E.Y., and Eisenberg, E. (2020). The cell line A-to-I RNA editing catalogue. *Nucleic Acids Res.* 48, 5849–5858. <https://doi.org/10.1093/nar/gkaa305>.
 36. Licht, K., Kapoor, U., Mayrhofer, E., and Jantsch, M.F. (2016). Adenosine to Inosine editing frequency controlled by splicing efficiency. *Nucleic Acids Res.* 44, 6398–6408. <https://doi.org/10.1093/nar/gkw325>.
 37. Licht, K., Kapoor, U., Amman, F., Picardi, E., Martin, D., Bajad, P., and Jantsch, M.F. (2019). A high resolution A-to-I editing map in the mouse identifies editing events controlled by pre-mRNA splicing. *Genome Res.* 29, 1453–1463. <https://doi.org/10.1101/gr.242636.118>.
 38. Jaitin, D.A., Weiner, A., Yofe, I., Lara-Astiaso, D., Keren-Shaul, H., David, E., Salame, T.M., Tanay, A., van Oudenaarden, A., and Amit, I. (2016). Dissecting Immune Circuits by Linking CRISPR-Pooled Screens with Single-Cell RNA-Seq. *Cell* 167, 1883–1896.e15. <https://doi.org/10.1016/j.cell.2016.11.039>.
 39. Dixit, A., Parnas, O., Li, B., Chen, J., Fulco, C.P., Jerby-Arnon, L., Marjanovic, N.D., Dionne, D., Burks, T., Raychowdhury, R., et al. (2016). Perturb-Seq: Dissecting Molecular Circuits with Scalable Single-Cell RNA Profiling of Pooled Genetic Screens. *Cell* 167, 1853–1866.e17. <https://doi.org/10.1016/j.cell.2016.11.038>.
 40. Datlinger, P., Rendeiro, A.F., Schmidl, C., Krausgruber, T., Traxler, P., Klughammer, J., Schuster, L.C., Kuchler, A., Alpar, D., and Bock, C. (2017). Pooled CRISPR screening with single-cell transcriptome readout. *Nat. Methods* 14, 297–301. <https://doi.org/10.1038/nmeth.4177>.
 41. Xu, Z., Sziraki, A., Lee, J., Zhou, W., and Cao, J. (2024). Dissecting key regulators of transcriptome kinetics through scalable single-cell RNA profiling of pooled CRISPR screens. *Nat. Biotechnol.* 42, 1218–1223. <https://doi.org/10.1038/s41587-023-01948-9>.
 42. Hill, A.J., McFaline-Figueroa, J.L., Starita, L.M., Gasperini, M.J., Matreyek, K.A., Packer, J., Jackson, D., Shendure, J., and Trapnell, C. (2018). On the design of CRISPR-based single-cell molecular screens. *Nat. Methods* 15, 271–274. <https://doi.org/10.1038/nmeth.4604>.
 43. Tian, R., Abarrientos, A., Hong, J., Hashemi, S.H., Yan, R., Dräger, N., Leng, K., Nalls, M.A., Singleton, A.B., Xu, K., et al. (2021). Genome-wide CRISPRi/a screens in human neurons link lysosomal failure to ferroptosis. *Nat. Neurosci.* 24, 1020–1034. <https://doi.org/10.1038/s41593-021-00862-0>.
 44. La Manno, G., Soldatov, R., Zeisel, A., Braun, E., Hochgerner, H., Petukhov, V., Lidschreiber, K., Kastriti, M.E., Lönnberg, P., Furlan, A., et al. (2018). RNA velocity of single cells. *Nature* 560, 494–498. <https://doi.org/10.1038/s41586-018-0414-6>.
 45. Picardi, E., D'Erchia, A.M., Lo Giudice, C., and Pesole, G. (2017). REDI-portal: a comprehensive database of A-to-I RNA editing events in humans. *Nucleic Acids Res.* 45, D750–D757. <https://doi.org/10.1093/nar/gkw767>.
 46. Kim, D.D.Y., Kim, T.T.Y., Walsh, T., Kobayashi, Y., Matise, T.C., Buyske, S., and Gabriel, A. (2004). Widespread RNA editing of embedded alu elements in the human transcriptome. *Genome Res.* 14, 1719–1725. <https://doi.org/10.1101/gr.285504>.
 47. Peng, Z., Cheng, Y., Tan, B.C.M., Kang, L., Tian, Z., Zhu, Y., Zhang, W., Liang, Y., Hu, X., Tan, X., et al. (2012). Comprehensive analysis of RNA-Seq data reveals extensive RNA editing in a human transcriptome. *Nat. Biotechnol.* 30, 253–260. <https://doi.org/10.1038/nbt.2122>.
 48. Bazak, L., Haviv, A., Barak, M., Jacob-Hirsch, J., Deng, P., Zhang, R., Isaacs, F.J., Rechavi, G., Li, J.B., Eisenberg, E., and Levanon, E.Y. (2014). A-to-I RNA editing occurs at over a hundred million genomic sites, located in a majority of human genes. *Genome Res.* 24, 365–376. <https://doi.org/10.1101/gr.164749.113>.
 49. Replogle, J.M., Saunders, R.A., Pogson, A.N., Hussmann, J.A., Lenail, A., Guna, A., Mascibroda, L., Wagner, E.J., Adelman, K., Lithwick-Yanai, G., et al. (2022). Mapping information-rich genotype-phenotype

- landscapes with genome-scale Perturb-seq. *Cell* 185, 2559–2575.e28. <https://doi.org/10.1016/j.cell.2022.05.013>.
50. Lo Giudice, C., Tangaro, M.A., Pesole, G., and Picardi, E. (2020). Investigating RNA editing in deep transcriptome datasets with REDItools and REDIportal. *Nat. Protoc.* 15, 1098–1131. <https://doi.org/10.1038/s41596-019-0279-7>.
 51. Roth, S.H., Levanon, E.Y., and Eisenberg, E. (2019). Genome-wide quantification of ADAR adenosine-to-inosine RNA editing activity. *Nat. Methods* 16, 1131–1138. <https://doi.org/10.1038/s41592-019-0610-9>.
 52. Hirano, M., Galarza-Munoz, G., Nagasawa, C., Schott, G., Wang, L., Antonia, A.L., Jain, V., Yu, X., Widen, S.G., Briggs, F.B.S., et al. (2023). The RNA helicase DDX39B activates FOXP3 RNA splicing to control T regulatory cell fate. *eLife* 12, e76927. <https://doi.org/10.7554/eLife.76927>.
 53. Torkler, P., Sauer, M., Schwartz, U., Corbaciglu, S., Sommer, G., and Heise, T. (2024). LoDEI: a robust and sensitive tool to detect transcriptome-wide differential A-to-I editing in RNA-seq data. *Nat. Commun.* 15, 9121. <https://doi.org/10.1038/s41467-024-53298-y>.
 54. Picardi, E., Manzari, C., Mastropasqua, F., Aiello, I., D'Erchia, A.M., and Pesole, G. (2015). Profiling RNA editing in human tissues: towards the inosinome Atlas. *Sci. Rep.* 5, 14941. <https://doi.org/10.1038/srep14941>.
 55. Wang, I.X., So, E., Devlin, J.L., Zhao, Y., Wu, M., and Cheung, V.G. (2013). ADAR regulates RNA editing, transcript stability, and gene expression. *Cell Rep.* 5, 849–860. <https://doi.org/10.1016/j.celrep.2013.10.002>.
 56. Zhou, X., Mitra, R., Hou, F., Zhou, S., Wang, L., and Jiang, W. (2023). Genomic Landscape and Potential Regulation of RNA Editing in Drug Resistance. *Adv. Sci.* 10, e2207357. <https://doi.org/10.1002/advs.202207357>.
 57. Galarza-Munoz, G., Briggs, F.B.S., Evsukova, I., Schott-Lerner, G., Kennedy, E.M., Nyanhete, T., Wang, L., Bergamaschi, L., Widen, S.G., Tomaras, G.D., et al. (2017). Human Epistatic Interaction Controls IL7R Splicing and Increases Multiple Sclerosis Risk. *Cell* 169, 72–84.e13. <https://doi.org/10.1016/j.cell.2017.03.007>.
 58. Desterro, J.M.P., Keegan, L.P., Lafarga, M., Berciano, M.T., O'Connell, M., and Carmo-Fonseca, M. (2003). Dynamic association of RNA-editing enzymes with the nucleolus. *J. Cell Sci.* 116, 1805–1818. <https://doi.org/10.1242/jcs.00371>.
 59. Fleckner, J., Zhang, M., Valcárcel, J., and Green, M.R. (1997). U2AF65 recruits a novel human DEAD box protein required for the U2 snRNP-branchpoint interaction. *Genes Dev.* 11, 1864–1872. <https://doi.org/10.1101/gad.11.14.1864>.
 60. Luo, M.L., Zhou, Z., Magni, K., Christoforides, C., Rappaport, J., Mann, M., and Reed, R. (2001). Pre-mRNA splicing and mRNA export linked by direct interactions between UAP56 and Aly. *Nature* 413, 644–647. <https://doi.org/10.1038/35098106>.
 61. Perez-Calero, C., Bayona-Feliu, A., Xue, X., Barroso, S.I., Munoz, S., Gonzalez-Basallote, V.M., Sung, P., and Aguilera, A. (2020). UAP56/DDX39B is a major cotranscriptional RNA-DNA helicase that unwinds harmful R loops genome-wide. *Genes Dev.* 34, 898–912. <https://doi.org/10.1101/gad.336024.119>.
 62. Wisskirchen, C., Ludersdorfer, T.H., Müller, D.A., Moritz, E., and Pavlovic, J. (2011). The cellular RNA helicase UAP56 is required for prevention of double-stranded RNA formation during influenza A virus infection. *J. Virol.* 85, 8646–8655. <https://doi.org/10.1128/JVI.02559-10>.
 63. Shen, J., Zhang, L., and Zhao, R. (2007). Biochemical characterization of the ATPase and helicase activity of UAP56, an essential pre-mRNA splicing and mRNA export factor. *J. Biol. Chem.* 282, 22544–22550. <https://doi.org/10.1074/jbc.M702304200>.
 64. Chen, Y.G., and Hur, S. (2022). Cellular origins of dsRNA, their recognition and consequences. *Nat. Rev. Mol. Cell Biol.* 23, 286–301. <https://doi.org/10.1038/s41580-021-00430-1>.
 65. Ishak, C.A., Loo Yau, H., and De Carvalho, D.D. (2021). Spliceosome-Targeted Therapies Induce dsRNA Responses. *Immunity* 54, 11–13. <https://doi.org/10.1016/j.immuni.2020.12.012>.
 66. Bowling, E.A., Wang, J.H., Gong, F., Wu, W., Neill, N.J., Kim, I.S., Tyagi, S., Orellana, M., Kurley, S.J., Dominguez-Vidaña, R., et al. (2021). Spliceosome-targeted therapies trigger an antiviral immune response in triple-negative breast cancer. *Cell* 184, 384–403.e21. <https://doi.org/10.1016/j.cell.2020.12.031>.
 67. Estornes, Y., Toscano, F., Virard, F., Jacquemin, G., Pierrot, A., Vanberverliet, B., Bonnin, M., Lalaoui, N., Mercier-Gouy, P., Pachéco, Y., et al. (2012). dsRNA induces apoptosis through an atypical death complex associating TLR3 to caspase-8. *Cell Death Differ.* 19, 1482–1494. <https://doi.org/10.1038/cdd.2012.22>.
 68. Awasthi, S., Verma, M., Mahesh, A., K Khan, M.I., Govindaraju, G., Rajavelu, A., Chavali, P.L., Chavali, S., and Dhayalan, A. (2018). DDX49 is an RNA helicase that affects translation by regulating mRNA export and the levels of pre-ribosomal RNA. *Nucleic Acids Res.* 46, 6304–6317. <https://doi.org/10.1093/nar/gky231>.
 69. Qian, Y., Li, J., Zhao, S., Matthews, E.A., Adoff, M., Zhong, W., An, X., Yeo, M., Park, C., Yang, X., et al. (2022). Programmable RNA sensing for cell monitoring and manipulation. *Nature* 610, 713–721. <https://doi.org/10.1038/s41586-022-05280-1>.
 70. Qu, L., Yi, Z., Zhu, S., Wang, C., Cao, Z., Zhou, Z., Yuan, P., Yu, Y., Tian, F., Liu, Z., et al. (2019). Programmable RNA editing by recruiting endogenous ADAR using engineered RNAs. *Nat. Biotechnol.* 37, 1059–1069. <https://doi.org/10.1038/s41587-019-0178-z>.
 71. Yi, Z., Zhao, Y., Yi, Z., Zhang, Y., Tang, G., Zhang, X., Tang, H., Zhang, W., Zhao, Y., Xu, H., et al. (2023). Utilizing AAV-mediated LEAPER 2.0 for programmable RNA editing in non-human primates and nonsense mutation correction in humanized Hurler syndrome mice. *Genome Biol.* 24, 243. <https://doi.org/10.1186/s13059-023-03086-6>.
 72. Wong, S.K., and Lazinski, D.W. (2002). Replicating hepatitis delta virus RNA is edited in the nucleus by the small form of ADAR1. *Proc. Natl. Acad. Sci. USA* 99, 15118–15123. <https://doi.org/10.1073/pnas.232416799>.
 73. Jayan, G.C., and Casey, J.L. (2002). Increased RNA editing and inhibition of hepatitis delta virus replication by high-level expression of ADAR1 and ADAR2. *J. Virol.* 76, 3819–3827. <https://doi.org/10.1128/jvi.76.8.3819-3827.2002>.
 74. Hsu, C.W., Juang, H.H., Kuo, C.Y., Li, H.P., Lang, S.B., Lin, S.H., Yeh, C.T., and Chao, M. (2019). Structural Pattern Differences in Unbranched Rod-like RNA of Hepatitis Delta Virus affect RNA Editing. *Viruses* 11, 934. <https://doi.org/10.3390/v11100934>.
 75. Wu, S., Xue, Q., Yang, M., Wang, Y., Kim, P., Zhou, X., and Huang, L. (2023). Genetic control of RNA editing in neurodegenerative disease. *Brief. Bioinform.* 24, bbad007. <https://doi.org/10.1093/bib/bbad007>.
 76. Sapiro, A.L., Freund, E.C., Restrepo, L., Qiao, H.H., Bhate, A., Li, Q., Ni, J.Q., Mosca, T.J., and Li, J.B. (2020). Zinc Finger RNA-Binding Protein Zn72D Regulates ADAR-Mediated RNA Editing in Neurons. *Cell Rep.* 31, 107654. <https://doi.org/10.1016/j.celrep.2020.107654>.
 77. Chen, P.J., Hussmann, J.A., Yan, J., Knipping, F., Ravisankar, P., Chen, P.F., Chen, C., Nelson, J.W., Newby, G.A., Sahin, M., et al. (2021). Enhanced prime editing systems by manipulating cellular determinants of editing outcomes. *Cell* 184, 5635–5652.e29. <https://doi.org/10.1016/j.cell.2021.09.018>.
 78. Yan, J., Oyler-Castrillo, P., Ravisankar, P., Ward, C.C., Levesque, S., Jing, Y., Simpson, D., Zhao, A., Li, H., Yan, W., et al. (2024). Improving prime editing with an endogenous small RNA-binding protein. *Nature* 628, 639–647. <https://doi.org/10.1038/s41586-024-07259-6>.
 79. Fang, L., Wang, W., Li, G., Zhang, L., Li, J., Gan, D., Yang, J., Tang, Y., Ding, Z., Zhang, M., et al. (2020). CIGAR-seq, a CRISPR/Cas-based method for unbiased screening of novel mRNA modification regulators. *Mol. Syst. Biol.* 16, e10025. <https://doi.org/10.1525/msb.202010025>.
 80. Kowalski, M.H., Wessels, H.H., Linder, J., Dalgarno, C., Mascio, I., Choudhary, S., Hartman, A., Hao, Y., Kundaje, A., and Satija, R. (2024). Multiplexed single-cell characterization of alternative polyadenylation

- regulators. *Cell* 187, 4408–4425.e23. <https://doi.org/10.1016/j.cell.2024.06.005>.
81. Booth, K.T.A., Jangam, S.V., Chui, M.M.C., Treat, K., Graziani, L., Solodano, A., Ruan, Y., Wan-Hei Hui, J., White, K., Christensen, C.K., et al. (2025). De novo and inherited variants in DDX39B cause a novel neurodevelopmental syndrome. *Brain*, awaf035. <https://doi.org/10.1093/brain/awaf035>.
 82. Zhao, G., Yuan, H., Li, Q., Zhang, J., Guo, Y., Feng, T., Gu, R., Ou, D., Li, S., Li, K., and Lin, P. (2022). DDX39B drives colorectal cancer progression by promoting the stability and nuclear translocation of PKM2. *Signal Transduct. Target. Ther.* 7, 275. <https://doi.org/10.1038/s41392-022-01096-7>.
 83. Zhang, H., He, C., Guo, X., Fang, Y., Lai, Q., Wang, X., Pan, X., Li, H., Qin, K., Li, A., et al. (2022). DDX39B contributes to the proliferation of colorectal cancer through direct binding to CDK6/CCND1. *Cell Death Discov.* 8, 30. <https://doi.org/10.1038/s41420-022-00827-7>.
 84. Feng, T., Li, S., Zhao, G., Li, Q., Yuan, H., Zhang, J., Gu, R., Ou, D., Guo, Y., Kou, Q., et al. (2023). DDX39B facilitates the malignant progression of hepatocellular carcinoma via activation of SREBP1-mediated de novo lipid synthesis. *Cell. Oncol.* 46, 1235–1252. <https://doi.org/10.1007/s13402-023-00807-8>.
 85. Chen, T., Chen, X., Zhang, S., Zhu, J., Tang, B., Wang, A., Dong, L., Zhang, Z., Yu, C., Sun, Y., et al. (2021). The Genome Sequence Archive Family: Toward Explosive Data Growth and Diverse Data Types. *Genom. Proteom. Bioinform.* 19, 578–583. <https://doi.org/10.1016/j.gpb.2021.08.001>.
 86. CNCB-NGDC Members and Partners (2022). Database Resources of the National Genomics Data Center, China National Center for Bio-information in 2022. *Nucleic Acids Res.* 50, D27–D38. <https://doi.org/10.1093/nar/gkab951>.
 87. Dobin, A., Davis, C.A., Schlesinger, F., Drenkow, J., Zaleski, C., Jha, S., Batut, P., Chaisson, M., and Gingeras, T.R. (2013). STAR: ultrafast universal RNA-seq aligner. *Bioinformatics* 29, 15–21. <https://doi.org/10.1093/bioinformatics/bts635>.
 88. Wolf, F.A., Angerer, P., and Theis, F.J. (2018). SCANPY: large-scale single-cell gene expression data analysis. *Genome Biol.* 19, 15. <https://doi.org/10.1186/s13059-017-1382-0>.
 89. Mansi, L., Tangaro, M.A., Lo Giudice, C., Flati, T., Kopel, E., Schaffer, A., Castrignanò, T., Chillemi, G., Pesole, G., and Picardi, E. (2021). REDI-portal: millions of novel A-to-I RNA editing events from thousands of RNAseq experiments. *Nucleic Acids Res.* 49, D1012–D1019. <https://doi.org/10.1093/nar/gkaa916>.
 90. Sherry, S.T., Ward, M.H., Kholodov, M., Baker, J., Phan, L., Smigelski, E. M., and Sirotkin, K. (2001). dbSNP: the NCBI database of genetic variation. *Nucleic Acids Res.* 29, 308–311. <https://doi.org/10.1093/nar/29.1.308>.
 91. Badia-I-Mompel, P., Vélez Santiago, J., Braunger, J., Geiss, C., Dimitrov, D., Müller-Dott, S., Taus, P., Dugourd, A., Holland, C.H., Ramirez Flores, R.O., and Saez-Rodriguez, J. (2022). decoupleR: ensemble of computational methods to infer biological activities from omics data. *Bioinform. Adv.* 2, vbac016. <https://doi.org/10.1093/bioadv/vbac016>.
 92. Muzellec, B., Telenczuk, M., Cabeli, V., and Andreux, M. (2023). PyDESeq2: a python package for bulk RNA-seq differential expression analysis. *Bioinformatics* 39, btad547. <https://doi.org/10.1093/bioinformatics/btad547>.
 93. Wang, Y., Wei, T., Zhao, M., Huang, A., Sun, F., Chen, L., Lin, R., Xie, Y., Zhang, M., Xu, S., et al. (2024). Alkenyl oxindole is a novel PROTAC moiety that recruits the CRL4DCAF11 E3 ubiquitin ligase complex for targeted protein degradation. *PLoS Biol.* 22, e3002550. <https://doi.org/10.1371/journal.pbio.3002550>.
 94. Wei, T., Lin, R., Fu, X., Lu, Y., Zhang, W., Li, Z., Zhang, J., and Wang, H. (2022). Epigenetic regulation of the DNMT1/MT1G/KLF4/CA9 axis synergises the anticancer effects of sorafenib in hepatocellular carcinoma. *Pharmacol. Res.* 180, 106244. <https://doi.org/10.1016/j.phrs.2022.106244>.
 95. Frankish, A., Carbonell-Sala, S., Diekhans, M., Jungreis, I., Loveland, J. E., Mudge, J.M., Sisu, C., Wright, J.C., Arnan, C., Barnes, I., et al. (2023). GENCODE: reference annotation for the human and mouse genomes in 2023. *Nucleic Acids Res.* 51, D942–D949. <https://doi.org/10.1093/nar/gkac1071>.
 96. Tarailo-Graovac, M., and Chen, N. (2009). Using RepeatMasker to identify repetitive elements in genomic sequences. *Curr. Protoc. Bioinformatics Chapter 4*, 4 10 11–14 10 14. <https://doi.org/10.1002/0471250953.bi0410s25>.
 97. Wang, K., Li, M., and Hakonarson, H. (2010). ANNOVAR: functional annotation of genetic variants from high-throughput sequencing data. *Nucleic Acids Res.* 38, e164. <https://doi.org/10.1093/nar/gkq603>.
 98. Li, H., Handsaker, B., Wysoker, A., Fennell, T., Ruan, J., Homer, N., Marth, G., Abecasis, G., and Durbin, R.; 1000 Genome Project Data Processing Subgroup (2009). The Sequence Alignment/Map format and SAMtools. *Bioinformatics* 25, 2078–2079. <https://doi.org/10.1093/bioinformatics/btp352>.
 99. Schindelin, J., Arganda-Carreras, I., Frise, E., Kaynig, V., Longair, M., Pietzsch, T., Preibisch, S., Rueden, C., Saalfeld, S., Schmid, B., et al. (2012). Fiji: an open-source platform for biological-image analysis. *Nat. Methods* 9, 676–682. <https://doi.org/10.1038/nmeth.2019>.
 100. Stirling, D.R., Swain-Bowden, M.J., Lucas, A.M., Carpenter, A.E., Cimini, B.A., and Goodman, A. (2021). CellProfiler 4: improvements in speed, utility and usability. *BMC Bioinf.* 22, 433. <https://doi.org/10.1186/s12859-021-04344-9>.

STAR★METHODS

KEY RESOURCES TABLE

REAGENT or RESOURCE	SOURCE	IDENTIFIER
Antibodies		
Rabbit monoclonal anti-ADAR1	Cell Signaling Technology	Cat#81284S; RRID:AB_3068597
Mouse monoclonal anti-DYKDDDDK (HRP)	Absin Bioscience	Cat#abs830014; RRID:AB_3683650
Rabbit monoclonal anti-HA	Cell Signaling Technology	Cat#3724; RRID:AB_1549585
Rabbit monoclonal anti-UAP56 (DDX39B)	Abcam	Cat#ab181061; RRID:AB_3683651
Mouse monoclonal anti-ADAR2	Santa Cruz Biotechnology	Cat#sc-73409; RRID:AB_2289194
Mouse monoclonal anti-SC35	Abcam	Cat#ab11826; RRID:AB_298608
Mouse monoclonal anti-dsRNA, clone rJ2	Millipore	Cat#MABE1134; RRID:AB_2819101
Mouse monoclonal anti-dsRNA	SCICONS	Cat#10010200; RRID:AB_2651015
Mouse monoclonal anti-HDAg	Kerafast	Cat#EHD001; RRID:AB_3696045
Bacterial and virus strains		
HDV infectious clone ZZ173	This paper	N/A
Stbl3 chemically competent E. coli	ALPALIFEBO	Cat#KTSMCC1200
Chemicals, peptides, and recombinant proteins		
DMEM	Thermo Fisher Scientific	Cat#C11995500BT
DMEM/F12	Thermo Fisher Scientific	Cat#C11330500BT
Opti-MEM I Reduced Serum Medium	GIBCO	Cat#31985070
Polyethylenimine Linear (PEI) MW40000	Yeasen	Cat#40816ES03
Lipofectamine RNAiMax Reagent	Invitrogen	Cat#13778150
Puromycin solution	Yeasen	Cat#60209ES50
RNase A	Yeasen	Cat#10406ES03
DAPI	Beyotime	Cat#C1006
Critical commercial assays		
MolPure® Cell RNA Kit	Yeasen	Cat#19231ES50
Chip A Single Cell Kit v2.1	MobiDrop	Cat#S050100301
High Throughput Single-Cell 3' Transcriptome Kit v2.1	MobiDrop	Cat# S050200301
3' Dual Index Kit	MobiDrop	Cat# S050300301
Easy II Protein Quantitative Kit	TransGen	Cat# DQ111
Deposited data		
Raw bulk RNA-seq and scRNA-seq data	This paper	GSA-Human: HRA011402
Processed data	This paper	Zenodo: https://doi.org/10.5281/zenodo.1529599
Experimental models: cell lines		
HEK293T	ATCC	Cat#CRL-3216
CRISPRi- HEK293T	This paper	N/A
CRISPRi- HEK293T-ADAR2	This paper	N/A
HepG2-NTCP	This paper	N/A
Oligonucleotides		
See Tables S2 and S3	NA	N/A
Recombinant DNA		
CREDITS vector	This paper	N/A
pLV2-UBC-mCherry-Hyg-CMV-ADAR2	This paper	N/A
pMK1334	Addgene	Cat#127965

(Continued on next page)

Continued

REAGENT or RESOURCE	SOURCE	IDENTIFIER
pcDNA3.1-3×Flag-ADAR1	This paper	N/A
pcDNA3.1-3×Flag-ADAR2	This paper	N/A
pcDNA3.1-3×HA-DDX39B	This paper	N/A
PX459	Addgene	Cat#62988
HDV dual-fluorescent RNA editing reporter	This paper	N/A
Software and algorithms		
MAGECK-iNC	Tian et al. ³³	https://kampmannlab.ucsf.edu/mageck-inc
GraphPad Prism 10	GraphPad	https://www.graphpad.com/
Fiji	NIH	https://fiji.sc/
PyMOL Molecular Graphics System Version 3.0	Schrödinger	https://pymol.org/
CellProfiler	Cimini Lab	https://cellprofiler.org/
STARsolo (STAR v2.7.11a)	Dobin et al. ⁸⁷	N/A
scnpy package (version 1.10.2)	Wolf et al. ⁸⁸	N/A
REDIportal	Mansi et al. ⁸⁹	http://srv00.recas.ba.infn.it/atlas/index.html
dbSNP (version v156)	Sherry et al. ⁹⁰	NA
decoupleR (version 1.8.0)	Badia et al. ⁹¹	https://www.bioconductor.org/packages/release/bioc/html/decoupleR.html
PyDESeqE (version 0.4.12)	Muzellec et al. ⁹²	https://github.com/owkin/PyDESeq2
SnapGene (version 8.0)	SnapGene	https://www.snapgene.com/
Code for scCREDITS analysis	This paper	https://doi.org/10.5281/zenodo.15614476

EXPERIMENTAL MODEL AND STUDY PARTICIPANT DETAILS

Cell culture

HEK293T, HuH7, and SH-SY5Y cells were purchased from ATCC and cultured in Dulbecco's Modified Eagle's Medium and DMEM/F12 (Gibco) supplemented with 10% fetal bovine serum (TransGen) and 1% penicillin and streptomycin (Aladdin). iPSC was cultured and differentiated into neurons as described previously.^{33,43} HepG2-NTCP cells were cultured in DMEM supplemented with 10% fetal bovine serum (Sigma) and 1% penicillin and streptomycin (Sigma) and 2.5 µg/mL puromycin (MedChemExpress). All cells were maintained at 37°C and 5% CO₂. All cell lines were tested routinely to be mycoplasma free by MycAway Plus-Color One-Step Mycoplasma Detection Kit (Yeasen, 40612ES25).

HDV

The HDV infectious clone ZZ173 was generated by inserting a 1.1mer HDV genome into the pcDNA3.1 plasmid (kindly provided by professor Stephan Urban of Heidelberg University). For production of HDV, HuH7 cells were co-transfected with ZZ173 and a plasmid expressing HBV envelope proteins (pT7-HB2.7), and medium was changed every 2 days. Cell culture containing the viral particles were harvested on days 9, 11, 13, and 15 post transfection, and further concentrated using 10% PEG8000.

METHOD DETAILS

Plasmid and siRNA transfection

The plasmids were transfected into the cells by Polyethylenimine Linear (PEI) MW40000 (Yeasen, 40816ES03) according to the standard protocol. The siRNAs targeting DDX39B (General biosystems) were transfected into the cells in combination with Lipofectamine RNAiMax Reagent (Invitrogen, 13778150) and Opti-MEM (Gibco, 31985–062) medium at 20 nM as final working concentration. The targeting sequences of each siRNA were listed in Table S2.

Generation of CREDITS vector

Sequence flanking the Q/R conversion site of *GRIA2* (chr4:157336674-157337074, hg38) was amplified from HEK293T genomic DNA by PCR. The amplified product was instead into a CROP-seq vector pMK1334 (Addgene, 127965) by replacing original WPRE cassette between EcoRI and SalI sites using ClonExpress Ultra One Step Cloning Kit (Vazyme, C115).

Generation of CRISPRi-HEK293T cell line with the stable overexpression of ADAR2

CRISPRi-HEK293T cell line was generated as described previously.⁹³ The cDNA of human *ADARB1* was gifted from Dr. Hao Chen (SUSTech) and was subcloned together with a 3×FLAG tag into a pLV2-UBC-mCherry-Hyg-CMV-MCS vector (Miaoling, P36518) between BamHI and AgeI sites. The lentivirus was packaged using psPAX2 (Addgene, 12260) and pMD2.G (Addgene, #12259) plasmids as described previously.⁹⁴ 7 days post lentivirus transduction, mCherry-positive CRISPRi-HEK293T cells with ADAR2 overexpression was sorted by FACS (BD FACSAria SORP). The cell pool was cultured and enlarged and the ADAR2 overexpression efficiency was verified by qRT-PCR and WB. The CRISPRi-HEK293T-ADAR2 cells was integrated with CREDITS vector using lentivirus transduction for further experiments.

Detection of RNA editing in CREDITS vector by sanger sequencing

Total RNA from the cells with CREDITS was extracted by MolPure Cell RNA Kit (Yeasen, 19231ES50) and 1 µg RNA was reverse transcribed to cDNA using HiScript III RT SuperMix (Vazyme, R323) according to the manufacturer's instruction. To measure RNA editing level in CREDITS vector, the cDNA products were used as templates for PCR to amplify the fragments flanking the A-to-I editing site and the PCR products were subjected to sanger sequencing. The abundance of nucleotide A and G in sequencing results was determined in SnapGene software and the RNA editing level was defined as the percentage of G/(A + G).

CRISPRi screening with CREDITS and data analysis

To integrate CREDITS vector with a human RNA binding protein (RBP) sgRNA library, 6,853 unique sgRNA sequences targeting 1,350 RBPs along with 250 non-targeting control sgRNAs, was synthesized by GENEWIZ and cloned into CREDITS vector between BstXI and BsplI sites. To evaluate the library quality, the fragment harboring sgRNA sequence was amplified using Phanta Flash Master Mix (Vazyme, P520) as manufacturer's instructions, and the PCR products were processed by next-generation sequencing (NGS).

For lentivirus production of the CREDITS vector integrated with RBP library, 5×10^6 HEK293T cells were plated onto a 15cm dish for 24 h before transfection. 15 µg library plasmid and 15 µg PackageMix plasmid were transfected into the HEK293T cells using Polyethylenimine Linear (PEI) MW40000 (Yeasen, 40816ES03). The PackageMix was prepared as an equal ratio mixture of three plasmids, including pMDLg/pRRE (Addgene, 12251), pRSV-Rev (Addgene, 12253), and pMD2.G (Addgene, 12259). 48 h later, the supernatant containing lentivirus was collected and filtered with a 0.45 µm filter (Millipore, SLHV033RB).

The lentivirus was transduced into CRISPRi-HEK293T-ADAR2 cells at 0.3 multiplicity of infection (MOI). 48 h later, the transduced cells were selected with 2 µg/mL of puromycin for 48 h to eliminate uninfected cells and generate a genome-edited cell pool. After 7-day passage in medium containing no puromycin, 10 million cells were collected for total RNA extraction by TRIzol reagent (Ambion). The mRNA containing poly-A tail from a total of 20 µg extracted RNA was reversed transcribed into cDNA using Oligo-dT primers by TransScript II One-Step gDNA Removal and cDNA Synthesis SuperMix (TransGen, AH311). All synthesized cDNA was used as template for PCR to amplify the linear region containing RNA editing reporter and sgRNA sequence. The PCR products were prepared for paired-end sequencing with Illumina platform (BerryGenomics). Raw FASTQ files for Read2 were cropped and aligned to the sgRNA reference of the RBP library using bowtie (v1.1.2) to identify sgRNAs, while Read1 files were cropped and aligned to a reference containing edited and unedited A-to-I reporter sequences to determine editing outcomes. This analysis enabled the determination of reporter editing levels for each identified sgRNA. Subsequently, the MAGeCK-iNC pipeline³³ was implemented to assess sgRNA-level and gene-level editing phenotypes as compared to non-targeting controls.

Primary validation of screening hits

Individual sgRNAs of top negative and positive hits in analysis results were cloned into the CREDITS vector via BstXI and BsplI sites. For lentivirus production of the CREDITS vector integrated with individual sgRNA, 1×10^5 HEK293T cells per well were plated onto a 12-well plate for 24 h before transfection. 0.5 µg CREDITS vector and 0.5 µg PackageMix plasmid were transfected into the HEK293T cells using PEI. The remaining procedures were performed as described above. 5-day post lentivirus transduction, the cells were collected for RNA extraction and the RNA editing level was determined as described in "Detection of RNA editing in CREDITS vector by sanger sequencing". The sgRNA sequences used in this study was listed in [Table S2](#).

Quantitative real-time PCR (qRT-PCR)

Total cellular RNA from cells was extracted using MolPure Cell RNA Kit (Yeasen, 19231ES50) following the manufacturer's instructions. cDNA was reverse transcribed from 1 µg RNA using HiScript III RT SuperMix for qPCR (Vazyme, R323). Quantitative real-time PCR was performed using Taq Pro Universal SYBR qPCR Master Mix (Vazyme, Q712) according to the manufacturer's protocol and ran on the LineGene 9600 Plus Real-Time PCR Detection System (Bioer, FQD-96A). Gene relative expression level was calculated using the $2^{-\Delta\Delta Ct}$ method, and *ACTB* was used as an endogenous control. The qRT-PCR primers used in this study are listed in [Table S4](#).

Immunoblotting

Cells were lysed in RIPA buffer (Beyotime, #P0013B) supplemented with phosphatase inhibitor cocktail (Selleck, B15001) and protease inhibitor cocktail (MCE, HY-K0010). The protein concentration of each sample was determined by Easy II Protein Quantitative Kit (TransGen, DQ111). Protein was denatured in loading buffer (Solarbio, P1041) by boiling at 95°C for 10 min, and 20 µg protein from

each lysate was electrophoresed on SDS-PAGE gels and was transferred to 0.45 μm PVDF membranes (Immobilon, IPVH00010). The membrane was blocked by 5% BSA (Sigma-Aldrich, V900933) in TBST (Sangon, C520009), and incubated with primary antibodies as indicated at 4°C overnight. Next day, the membrane was incubated with horseradish peroxidase-conjugated secondary antibodies for 1 h at room temperature. The protein signal was detected using the clarity western ECL substrate (EpiZyme, SQ202L). The tri-color pre-stained protein marker was used to indicate the molecular weights of protein bands (Shandong Sparkjade Biotechnology Co., Ltd. EC2019, EC1020). The antibodies used in this study are summarized here: anti-UAP56/DDX39B (Abcam, 181061), anti-ADAR1 (CST, 81284S), anti-Flag (Absin, abs830014), anti-HA (CST, 3724S).

Co-immunoprecipitation (Co-IP)

The experiment was performed as described previously.⁹⁴ In brief, 3×10^6 HEK293T cells were plated onto a 10cm diameter dish for 24 h before transfection. The pcDNA3.1-3×Flag-ADAR1 and pcDNA3.1-3×HA-DDX39B were transfected into the cells. 48 h later, the cells were collected and lysed in NP-40 buffer (Beyotime, P0013F). The cell lysates were centrifuged at 12,000 rpm at 4°C for 10 minutes, then the supernatant was collected and treated with 400 μg RNase A (Yeasen, 10406ES03) at room temperature for 2 min. Subsequently, the supernatant was incubated with anti-Flag magnetic beads (Beyotime, P2181S) at 4°C for 4 h. After washing, the beads affiliated with proteins were denatured and subjected to immunoblotting analysis.

scCREDIT-seq and data analysis

The overall scCREDIT-seq process was derived from CROP-seq as described previously.³³ In brief, CRISPRi-HEK293T cells with or without ADAR2 overexpression were transduced with individual lentivirus of selected sgRNAs in the CROP-seq vector pMK1334. After puromycin selection and expansion, all cells were pooled together at equal ratio. Approximately 20,000 cells were loaded into microfluidic chip of Chip A Single Cell Kit v2.1 (MobiDrop, S050100301) to generate droplets with MobiNova-100 (MobiDrop, A1A40001). Each cell was involved into a droplet which contained a gel bead linked with up to millions oligos (cell unique barcode). After encapsulation, droplets suffer light cut by MobiNovaSP-100 (MobiDrop, A2A40001) while oligos diffuse into reaction mix. The mRNAs were captured by cell barcodes with cDNA amplification in droplets. Following reverse transcription, cDNAs with barcodes were amplified, and a library was constructed using the High Throughput Single-Cell 3' Transcriptome Kit v2.1 (MobiDrop, S050200301) and the 3' Dual Index Kit (MobiDrop, S050300301).

To facilitate sgRNA assignment, sgRNA-containing transcripts were additionally amplified by hemi-nested PCR reactions as described previously.³³ The sgRNA-enrichment libraries were separately indexed and sequenced as spike-ins alongside the whole-transcriptome scRNA-seq libraries using NovaSeq 6000 system. The primers used for sgRNA enrichment PCR was listed in Table S3.

Processing of single-cell gene expression data

Single-cell RNA sequencing (scRNA-seq) and Feature Barcoding data from HEK293T cells were processed using STARsolo (STAR v2.7.11a).⁸⁷ Human genome GRCh38 and GENCODE v44 were used as ref.⁹⁵ The gRNA-amplified library data was analyzed and assigned to cell barcodes using customized Python3 scripts (available at <https://github.com/comics-bio/scCREDITS-seq>). The resulting count matrices and gRNA-cell barcode mapping matrices were then used as input for downstream analyses with the scanpy package (version 1.10.2).⁸⁸ We retained cells with unique sgRNA assignments and filtered out those that were not fully perturbed. To further refine our dataset, we excluded cells that may have received an sgRNA but did not exhibit strong molecular evidence of successful perturbation. Specifically, we retained only cells where the expression levels of target genes were below those of 75% of cells. Conversely, the cells with control sgRNA were required to have all target genes expressed in more than 85% of cells.

For visualization, we used Linear Discriminant Analysis (LDA), a supervised dimensionality reduction technique that identifies a low-dimensional subspace to maximize discrimination between different groups ('perturbations') in the data. Before applying LDA, we reduced the dimensionality of our dataset (editing index or expression matrix) to 108 features (6 projected principal components × 18 perturbations). The components returned from LDA were then used as input for 2D visualization with UMAP.

Single-cell metric for A-to-I RNA editing

We developed a single-cell metric for A-to-I RNA editing that adjusts for the total gene abundance to prioritize the detection of overall changes in RNA editing. We used only reads with a mapping quality greater than 255 and a base quality above 30 as input. Our analysis focused on known editing sites reported in REDIportal⁸⁹ and we excluded common A to G SNPs annotated in dbSNP (version v156).⁹⁰ Highly confident A-to-I sites were retained through a series of filtering steps. Specifically, we only kept sites that met all of the following criteria: (i) ≥ 2 edited reads across all cells; (ii) ≥ 10 reads (edited and unedited) across all cells; (iii) editing detected in $\geq 0.5\%$ of all cells; (iv) at the editing site, the number of cells with base C/T (noise) $< 20\%$ * the number of cells with base G (signal). The remaining sites were annotated with gene symbols using RefGene, repeat regions using RepeatMasker,⁹⁶ and known RNA editing sites using the REDIportal (V2)⁸⁹ via ANNOVAR (version 2020.06.07).⁹⁷ The cell editing index (CEI) is defined as below:

$$CEI_i = \frac{N_i * 1000}{U_i}$$

where:

CEI_i : Cell Editing Index for cell i .

N_i : Number of UMIs with at least one editing site in cell i .

U_i : Total UMI counts of cell i .

Z – score normalized CEI values were used for visualization.

Statistical testing for CEI between different sgRNA groups was performed using a t test, and Differential Expression Gene (DEG) analysis was conducted with the decoupleR (Version 1.8.0)⁹¹ and PyDESeqE (Version 0.4.12)⁹² with a pseudobulk stragecy.

RNA sequencing (RNA-seq) and data analysis

The CRISPRi-HEK293T cells with different gene perturbation by sgRNAs were collected and total RNA was extracted using TRIzol reagent (Ambion). The sgRNA sequences used in this experiment were listed in Table S2. RNA quantification and concentration was measured using Qubit 4.0 (Thermo Scientific). RNA integrity was assessed using Agilent 2100 Bioanalyzer (Agilent Technologies). RNA purity was controlled by NanoDrop.

A total amount of 500 ng RNA per sample was used as input material for the RNA sample preparations. Ribosomal RNA was removed from total RNA using Ribo-off rRNA Depletion Kit (Yeasen). Sequencing libraries were generated using HiSeq NGS Ultima Dual-mode mRNA Library Prep Kit for Illumina (Yeasen, 12301) following manufacturer's recommendations and index codes were added to attribute sequences to each sample. The library quality was assessed on the Qseq 100 system. The dsDNA library was denatured, cyclized, and digested to obtain single-stranded circular DNA, and DNB nanospheres were obtained by Rolling Circle Amplification (RCA). The prepared DNB was loaded onto a microarray chip (Patterned Array) and sequenced on DNBSEQ-T7 platform (Geneplus-Shenzhen) using Combinatorial Probe-Anchor Synthesis (cPAS), and 150 bp paired-end reads were generated.

All raw data were mapped to the GRCh38 genome assembly using GENCODE gene annotations v44 with STAR (v2.7.11a). The resulting BAM files for each sample were sorted with samtools⁹⁸ and used as input for RNAEditingIndexer (latest version)⁵¹ to assess sample RNA editing level. A-to-I RNA editing events and editing levels at known sites with coverage above ten reads were detected and queried using REDITools.⁵⁰ To minimize false positives, only editing sites included in REDIportal⁸⁹ were used for downstream analysis. Subsequently, all selected sites were annotated with ANNOVAR⁹⁷ to map gene symbols using RefGene and repeat regions using RepeatMasker⁹⁶ data. All downstream analyses were performed using customized Python3 scripts (<https://github.com/comics-bio/scCREDITS-seq>). The numbers of up- and down-regulated editing sites were calculated only for sites with an absolute log₂ fold change (|log₂FC|) greater than 0.5. For gene expression analysis, gene quantification was performed with RSEM (v1.3.1). The R package DESeq2 was then used to fit the expression count matrix to a negative binomial distribution and identify differentially expressed genes. Adjusted $p < 0.05$ and log₂ fold-change > 1 were used to determine statistical significance. Gene Set Enrichment Analysis (GSEA) was done with GSEAPY (version 1.1.3).

Correlation analysis

To evaluate the consistency between single-cell and bulk RNA-seq datasets, we generated a pseudo-bulk expression matrix from the single-cell RNA-seq data using decoupler (v1.8.0),⁹¹ and conducted differential expression analysis with pyDESeq2 (v0.5.0).⁹² The same analysis pipeline was applied to the bulk RNA-seq data for consistency. The resulting log₂ fold change values of differentially expressed genes were compared across both datasets. For RNA editing analysis, we first grouped the aligned single-cell BAM files based on the knockdown condition to generate a pseudo-bulk BAM file. We then split both the pseudo-bulk scRNA-seq BAM file and the bulk RNA-seq BAM file by chromosome (chr1-chr22). RNA editing levels for each chromosome were quantified using RNAEditingIndexer.⁵¹

To evaluate the relationship between RNA editing and gene expression in bulk RNA-seq, we first performed differential RNA editing analysis between sg $DDX39B$ and sgControl groups using the LoDEI method,⁵³ retaining only editing windows with a q-value < 0.1 . For each gene, we calculated the mean window editing index (wEI) from all associated editing windows to represent its RNA editing level. We then compared these values with log₂ fold changes in gene expression (calculated using pyDESeq2, v0.5.0).

mNeonGreen knock-in for DDX39B in HEK293T

The CRISPR/Cas9 system was used to generate engineer HEK293T cell line. sgRNA targeting the exon 1 of $DDX39B$ was cloned into PX459 (Addgene, #62988). Donor double-strand DNA (dsDNA) containing microhomology and mNeonGreen cassette was constructed. To generate mNeonGreen- $DDX39B$ endogenous tagged HEK293T, 2 μ g PX459 and donor dsDNA were transfected into HEK293T using PEI (Yeasen, 40816ES01). 48hrs later, HEK293T cells were treated with 2 μ g/mL puromycin for 72hrs. Green-fluorescent single cells were sorted into a 96-well plate by FACS (BD FACSAria SORP). One week later, homogeneous knock-in clones were verified by PCR and Sanger sequencing. The genotyping PCR primers were listed in Table S4.

Immunofluorescence (IF)

Cells were plated at 5×10^4 per well on sterilized, Matrigel-coated 12mm diameter round glass coverslips (CITOTEST, 10210012CE) in 24-well plates. Next day, cells were fixed with 4% paraformaldehyde (Beyotime, P0099) at room temperature for 15 min. After washing, cells were treated with 0.1% Triton X-100 (Coolaber, CT11451) in PBS (BBI, E607008) for 5 min, then the cells were blocked

with 3% BSA (Sigma-Aldrich, V900933) in PBS (BBI, E607008) for 30 min. The cells were incubated with primary antibodies as indicated at 4°C overnight. Next day, the primary antibodies were washed out and the secondary antibodies were applied to the cells at room temperature for 1 h. After washing, the nucleus was stained by DAPI (Beyotime, C1006) at room temperature for 10 min. Finally, coverslips were then washed three times with PBS for 5 min each. One drop of Mounting Medium (SouthernBiotech, 0100) was added to the coverslips and the coverslips were sealed with slides (CITOTEST, 10127105P). The antibodies used in this study were listed here: anti-ADAR1 (CST, 81284S), anti-ADAR2 (SANTA CRUZ BIOTECHNOLOGY, sc-73409), anti-SC35 (Abcam, ab11826), anti-HDAg (FD3A7 clone, Kerafast, EHD001). The images were captured in a confocal microscope (Zeiss, LSM 980), and the protein colocalization analysis was performed by Fiji.⁹⁹

Detection of dsRNA accumulation

To detect the dsRNA accumulation by IF, cells were treated as described above in “Immunofluorescence (IF)”. The J2 antibody (Merck, MABE1134) specifically recognizes dsRNA was used in this experiment. The images were captured in a confocal microscope (Nikon) and subjected to the deconvolution processing using default setting. The fluorescent intensity of dsRNA was quantified using CellProfiler.¹⁰⁰

To detect the dsRNA accumulation by flow cytometry, cells were detached with 0.5 mM EDTA (LABSELECT, BL518A) and then washed twice using PBS. Cells were fixed with 4% paraformaldehyde (Beyotime, P0099) at room temperature for 20 min. After washing, cells were permeabilized with 0.1% Triton X-100 (Coolaber, CT11451) in PBS for 15 min followed by incubation in 3% BSA in PBS for 30 min, then the cells were stained with J2 antibody (SCICONS, 10010200) for 1 h at ice and secondary antibody for 30 min at room temperature. The dsRNA intensity was measured using flow cytometry (BD FACSCanto SORP).

Protein structure analysis and site mutagenesis

The crystal structure of DDX39B complexed with ADP and Magnesium ion was downloaded from PDB dataset (PDBid: 1xtj) and was analyzed using The PyMOL Molecular Graphics System Version 3.0 (Schrödinger). The site mutations of K95A, D197A, and E199A were introduced to wild-type DDX39B plasmid by homogeneous recombination. The primers were designed as listed in [Table S4](#).

Generation of CellREADR vector and data analysis

The CellREADR vector was generated by adapting a previously published article.⁶⁹ Briefly, the sequence of sense–edit–switch RNA (sesRNA) was synthesized by Tsingke and was inserted into FUW vector (Addgene, 14882) with mCherry and EGFP fragments using ClonExpress Ultra One Step Cloning Kit (Vazyme, C115). The sesRNA sequences and primers used in this study were listed in [Tables S3](#) and [S4](#), respectively.

The CellREADR vector was transfected into the cells using PEI. 72 h later, the cells were collected for flow cytometry analysis (BD FACSCanto SORP). The cell conversion ratio was defined as the percentage of mCherry⁺/EGFP⁺ double-positive cells over mCherry⁺ single-positive cells.

Generation of LEAPER vector and data analysis

The LEAPER vector was generated by adapting a previously published article.⁷⁰ In brief, the ADAR-recruiting RNAs (arRNA) was synthesized by Tsingke and was inserted into a pU6-pegRNA-GG-acceptor (Addgene, 132777) by replacing original mRFP1 cassette between dual Bsal sites. The hPGK promoter, puromycin resistance, EGFP, and SV40 poly(A) signal terminator were inserted to the vector using ClonExpress Ultra One Step Cloning Kit (Vazyme, C115).

The LEAPER vector was transfected into the cells using PEI. 72 h later, the EGFP positive cells were sorted by FACS (BD FACSAria SORP), and total RNA was extracted using MolPure Cell RNA Kit (Yeasen, 19231ES50). 500 ng RNA was reversed transcribed into cDNA using cDNA using Oligo-dT primers by TransScript II One-Step gDNA Removal and cDNA Synthesis SuperMix (TransGen, AH311). The cDNA products were used as templates for PCR to amplify the fragments flanking the A-to-I editing site and the PCR products were subjected to sanger sequencing or NGS. The abundance of nucleotide A and G in sequencing results was determined in SnapGene software and the RNA editing level was defined as the percentage of G/(A + G). The arRNA sequences and primers used in this study were listed in [Tables S3](#) and [S4](#), respectively.

HDV assays

The HDV infectious clone ZZ173 was generated by inserting a 1.1mer HDV genome into the pcDNA3.1 plasmid (kindly provided by professor Stephan Urban of Heidelberg University). For testing HDV genome editing in 293T cells, the plasmid and siRNAs were transiently transfected into the cells as described previously using PEI. Cells were harvested on days 5, 7, 9 post transfection. Total RNA was extracted using the FastPure Cell/Tissue Total RNA Isolation Kit (Vazyme, China). One microgram RNA of each sample was reverse transcribed using the HiScript III RT SuperMix (Vazyme, China). The cDNA products were used as templates for PCR to amplify the fragments flanking the A-to-I editing site and the PCR products were subjected to NGS. The primers used in this study were listed in [Table S4](#).

To generate HDV dual-fluorescent RNA editing reporter, the original sesRNA sequence in CellREADR vector was replaced by HDV HDAg sequence containing an ADAR-editable translation switch. 5-day post transfection, the fluorescent signal was detected and working efficiency was calculated as described above. The HDV HDAg sequence was listed in [Table S3](#).

For production of HDV, HuH7 cells were co-transfected with ZZ173 and a plasmid expressing HBV envelope proteins (pT7-HB2.7), and medium was changed every 2 days. Cell culture containing the viral particles were harvested on days 9, 11, 13, and 15 post transfection, and further concentrated using 10% PEG8000.

For testing the effect of DDX39B knockdown on HDV replication, HepG2-NTCP cells were seeded into 24-well plates, and siRNA transfection was performed during cell seeding. Cells were infected with HDV on day 1 post siRNA transfection in the presence of 4% PEG8000 and 2% DMSO. The viral inoculum was replaced with fresh medium containing 2% DMSO at 16 h post infection. On day 5 post infection, cells were harvested and HDV replication was measured by qRT-PCR of HDV RNA and IF of HDAg.

QUANTIFICATION AND STATISTICAL ANALYSIS

All data were statistically analyzed with GraphPad Prism 10 software. Data were presented as means \pm standard error of the mean (SEM). The criteria for statistical differences were: ns (not significant), $p > 0.05$, $*p < 0.05$, $**p < 0.01$, $***p < 0.001$, $****p < 0.0001$; and all of the sample size and the statistical details for each quantification can be found in the figure legends.